CHAPTER IV
RESULTS AND DISCUSSION

IV.1. Water retention function

Water retention function of tested soils used in the present study was expressed using two hydraulic models; van Genuchten-Mualem type function model **(van Genuchten, 1980)** and Durner multimodal pore system **(Durner *et al.*, 1999).** The results are reported in Tables (5 to 10) and Figures (7 to 12).

Table (5). van Genuchten soil parameters of Sandy loam soil(single pore system)

Soil Parameter	Sandy loam soil
θ_r (cm^3 cm^{-3})	0.0621
θ_s (cm^3 cm^{-3})	0.4229
α (cm^{-1})	0.0193
n	1.6176
m=(1-1/n)	0.3818
K_s (cm min^{-1})	0.074
R^2	0.9957

Table (6). van Genuchten soil parameters of Sandy soil (single pore system)

Soil Parameter	Sandy soil
θ_r (cm^3 cm^{-3})	0.0307
θ_s (cm^3 cm^{-3})	0.3661
α (cm^{-1})	0.0531
n	1.3621
m=(1-1/n)	0.2659
K_s (cm min^{-1})	0.356
R^2	0.9983

Table (7). van Genuchten soil parameters of Sandy clay loam soil (single pore system)

Soil Parameter	Sandy clay loam soil
θ_r (cm^3 cm^{-3})	0.0859
θ_s (cm^3 cm^{-3})	0.3920
α (cm^{-1})	0.0021
n	1.9768
m=(1-1/n)	0.4941
K_s (cm min^{-1})	0.022
R^2	0.9807

Table (8). Soil parameters of Durner's multimodal pore system for Sandy loam soil

Soil Parameters	Sandy loam soil
θ_r (cm^3 cm^{-3})	0.0001
θ_s (cm^3 cm^{-3})	0.4210
$\alpha 1$ (cm^{-1})	0.0096
n1	4.3714
m1	1.3972
w1	0.4191
$\alpha 2$ (cm^{-1})	0.0191
n2	2.6083
m2	0.0860
w2	0.5809
K_s (cm min^{-1})	0.074
R^2	0.9987

Table (9). Soil parameters of Durner's multimodal pore system for Sandy soil

Soil Parameters	Sandy soil
θ_r (cm^3 cm^{-3})	0.0558
θ_s (cm^3 cm^{-3})	0.3667
$\alpha 1$ (cm^{-1})	0.0023
n1	0.6490
m1	2.4500
w1	0.9125
$\alpha 2$ (cm^{-1})	0.0001
n2	4.4210
m2	1.0122
w2	0.0875
K_s (cm min^{-1})	0.356
R^2	0.9998

Table (10). Soil parameters of Durner's multimodal pore system for Sandy clay loam soil

Soil Parameters	Sandy clay loam soil
θ_r (cm^3 cm^{-3})	0.0783
θ_s (cm^3 cm^{-3})	0.3865
$\alpha 1$ (cm^{-1})	0.0250
n1	1.8226
m1	11.2294
w1	0.13
$\alpha 2$ (cm^{-1})	0.0024
n2	48.1183
m2	0.0161
w2	0.87
K_s (cm min^{-1})	0.022
R^2	0.9854

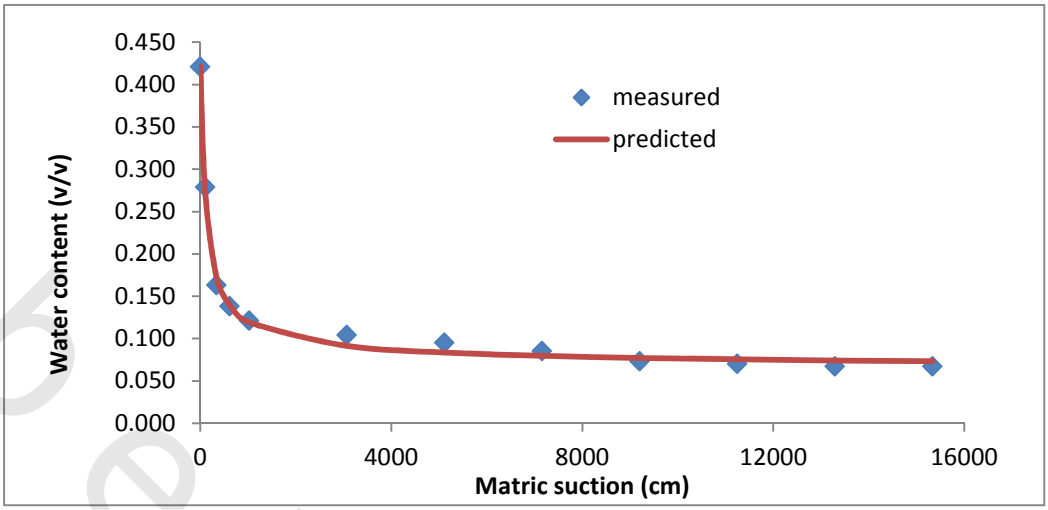

Fig. (7). Soil water retention curve of sandy loam soil (van Genuchten model)

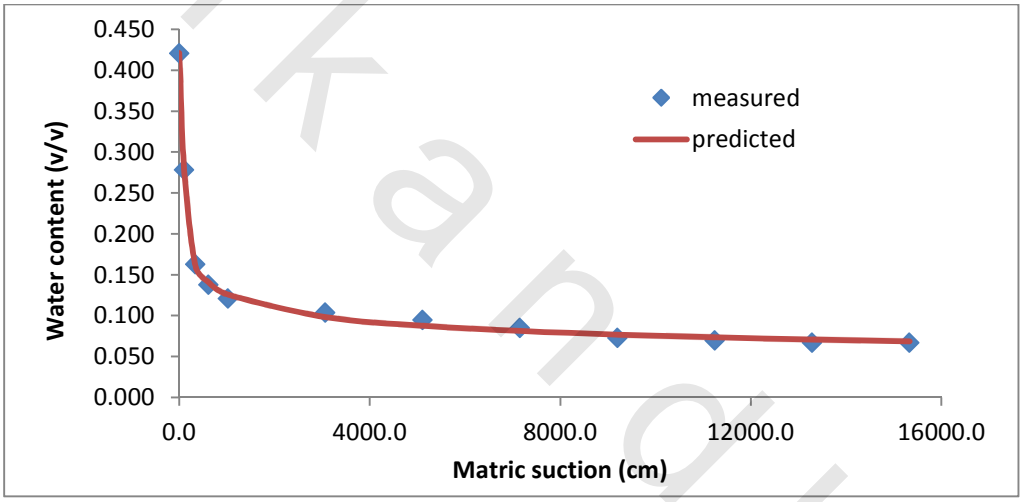

Fig. (8). Soil water retention curve of sandy loam soil (Durner's multimodal pore system)

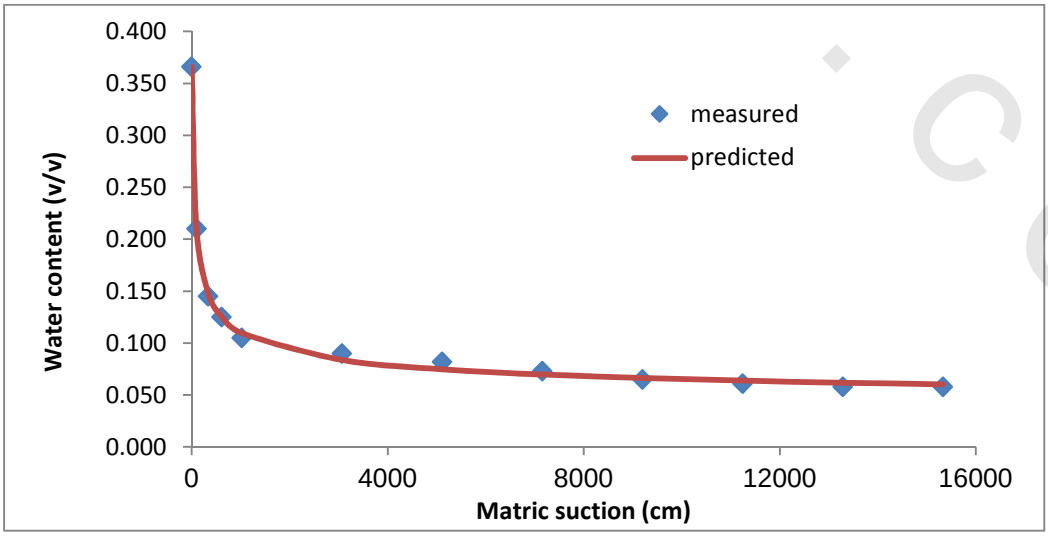

Fig. (9). Soil water retention curve of sandy soil (van Genuchten model)

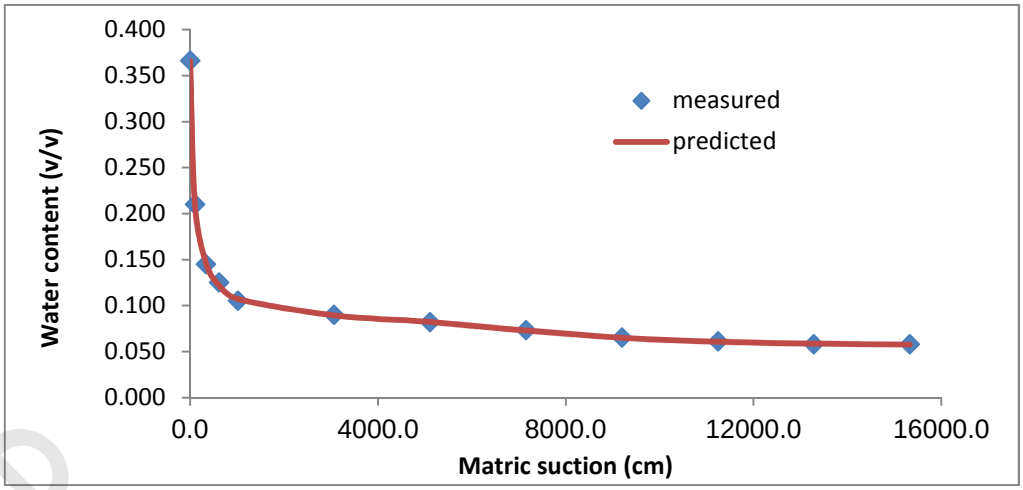

Fig. (10). Soil water retention curve of sandy soil (Durner's multimodal pore system)

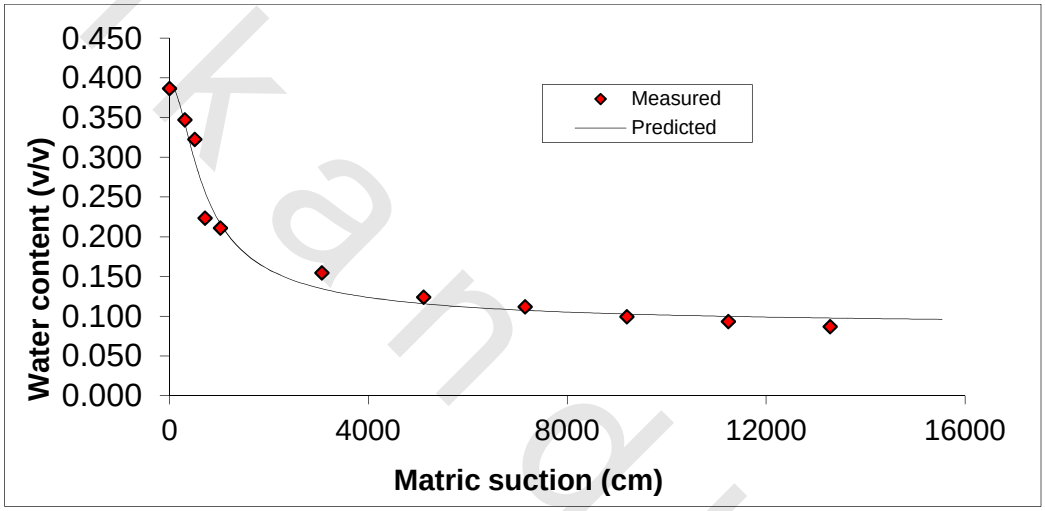

Fig. (11). Soil water retention curve of sandy clay loam soil (van Genuchten model)

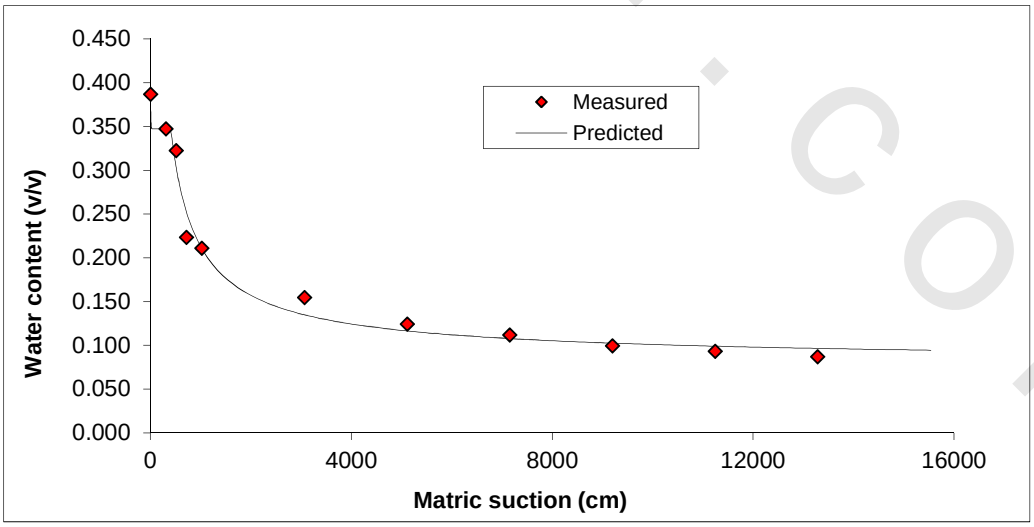

Fig. (12). Soil water retention curve of sandy clay loam soil (Durner's multimodal pore system)

IV.2. Potassium sorption isotherm

Potassium sorption isotherm was done according the method as described in **(Gazoly, 2002)** using linear sorption isotherm **(Šimůnek *et al*., 2013)** and two site sorption model **(Šimůnek *et al*., 2008).** The results are reported in Tables (11 to 13) and Figures (13 to 18).

Table (11). Potassium sorption parameters according to linear and Two-site sorption models for sandy loam soil

Sorption parameter	Sandy loam soil
Linear model:	
K_d	2.9552
R^2	0.9967
Two-site sorption model:	
K_d	2.9552
f_e	0.7000
R^2	0.9967

Table (12). Potassium sorption parameters according to linear and Two-site sorption models for sandy soil

Sorption parameter	Sandy soil
Linear model:	
K_d	1.7020
R^2	0.9931
Two-site sorption model:	
K_d	1.7020
f_e	0.8000
R^2	0.9931

Table (13). Potassium sorption parameters according to linear and Two-site sorption models for sandy clay loam soil

Sorption parameter	Sandy clay loam soil
Linear model:	
K_d	14.16
R^2	0.9935
Two-site sorption model:	
K_d	14.1642
f_e	0.7500
R^2	0.9935

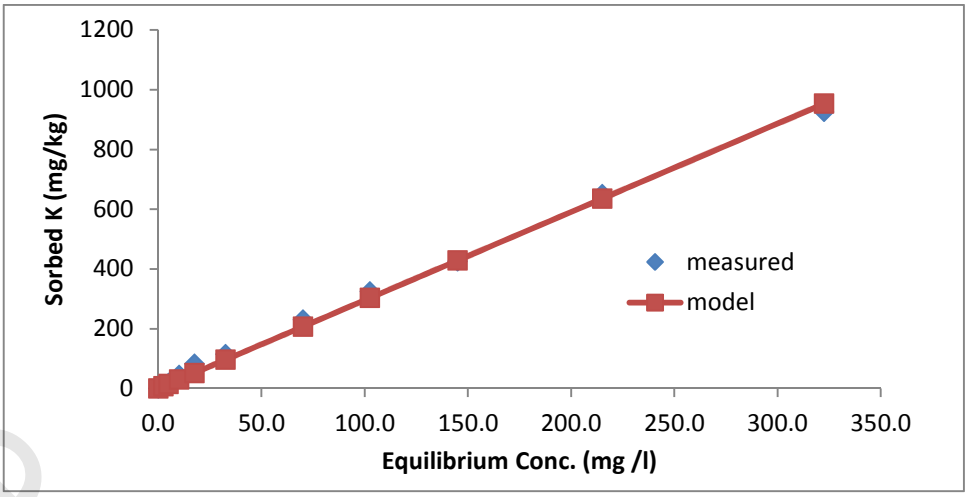

Fig. (13). Potassium sorption isotherm of sandy loam soil (linear model)

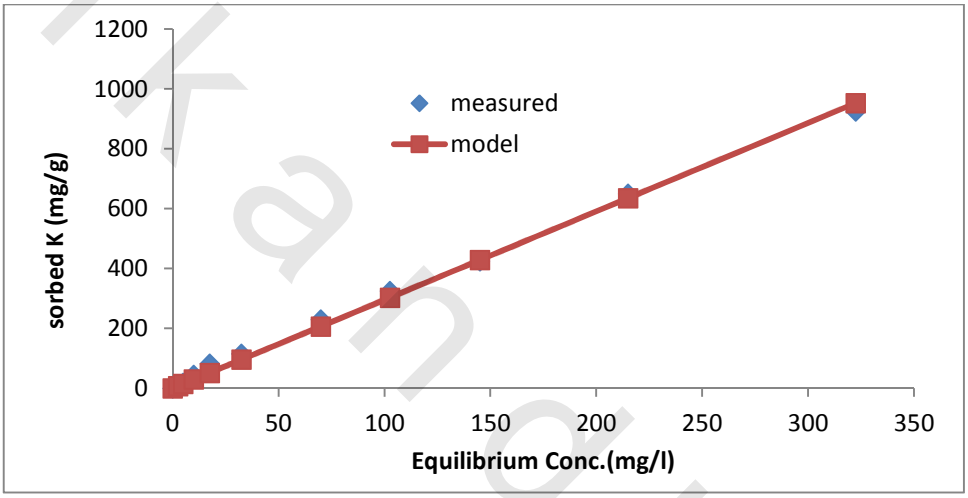

Fig. (14). Potassium sorption isotherm of sandy loam soil (two-site sorption model)

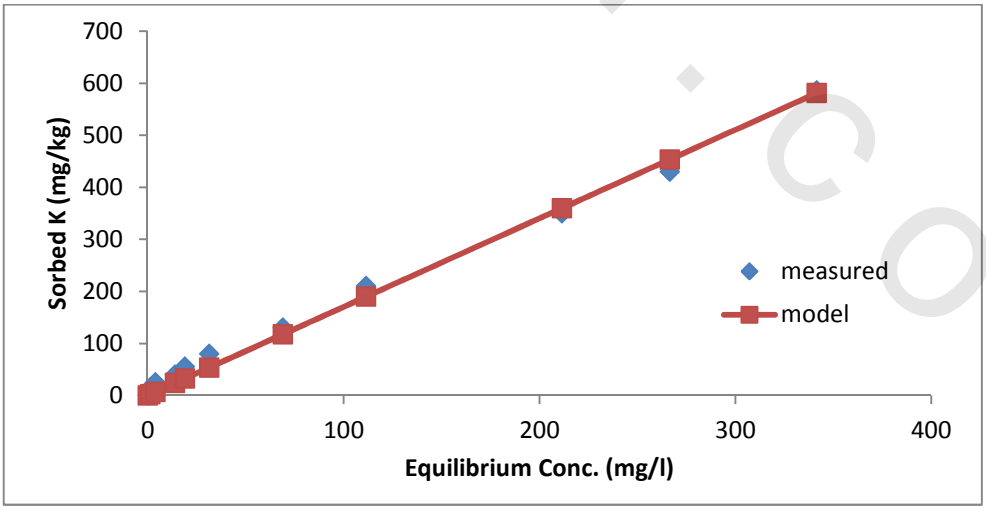

Fig. (15). Potassium sorption isotherm of sandy soil (linear model)

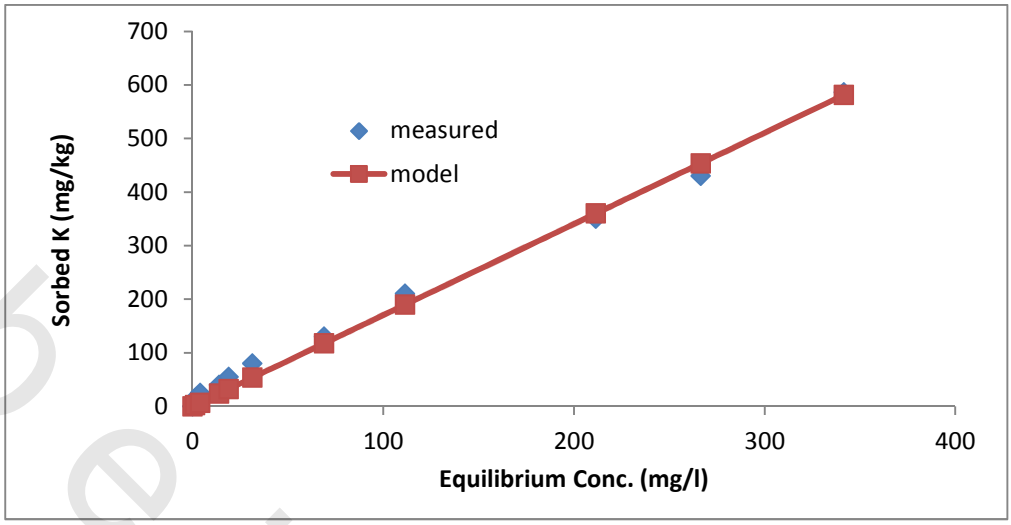

Fig. (16). Potassium sorption isotherm of sandy soil (two-site sorption model)

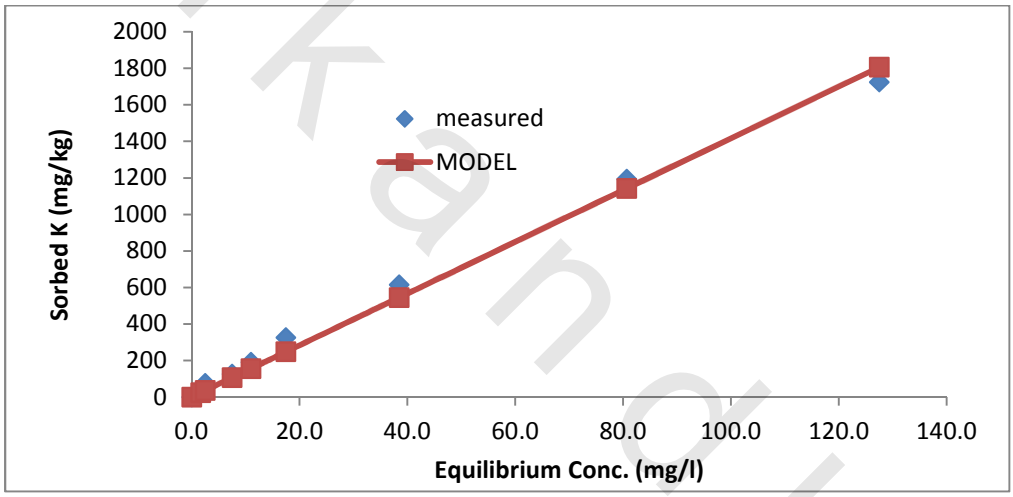

Fig. (17). Potassium sorption isotherm of sandy clay loam soil (linear model)

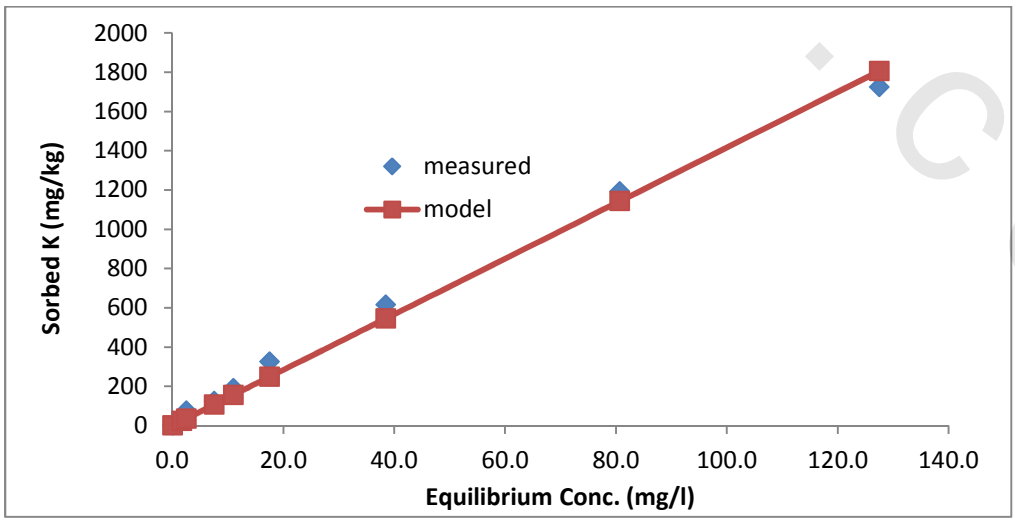

Fig. (18). Potassium sorption isotherm of sandy clay loam soil (two-site sorption model)

IV.3. Potassium transport with equilibrium and non-equilibrium models

IV.3.1. Sandy loam soil

Potassium transport through the soil column was done with applying some equilibrium and non-equilibrium transport models.

IV.3.1.1. Soil moisture distribution

Figures (19 to 21) show the moisture distribution in soil columns of sandy loam soil with different potassium application. The trend is uniform with low and high potassium application due to the same rate of solution application as 0.0233 cm/min. The distribution is differed with medium potassium application due to high solution application rate as 0.0454 cm/min. All cases reached to the same moisture content (0.409 cm^3 cm^{-3}).

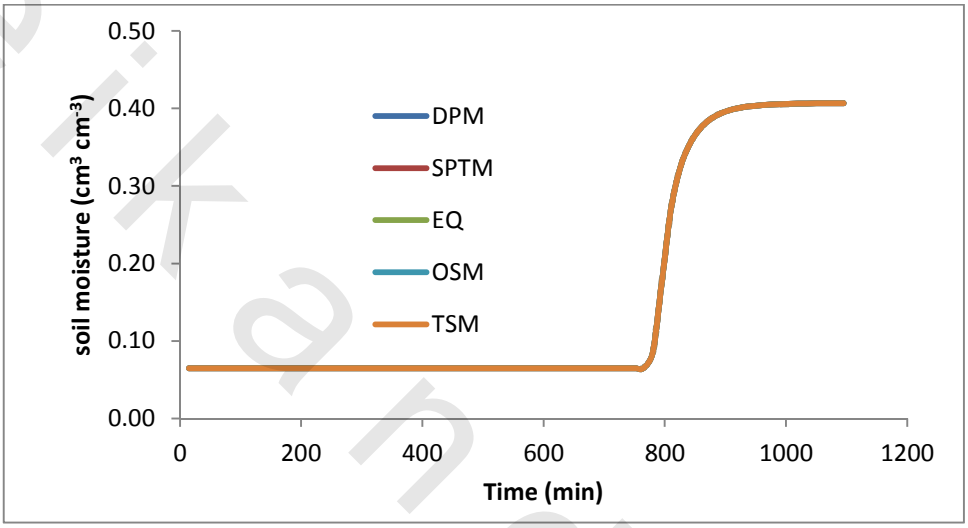

Fig. (19). Soil moisture distribution in soil column of sandy loam soil with low potassium application at different transport models

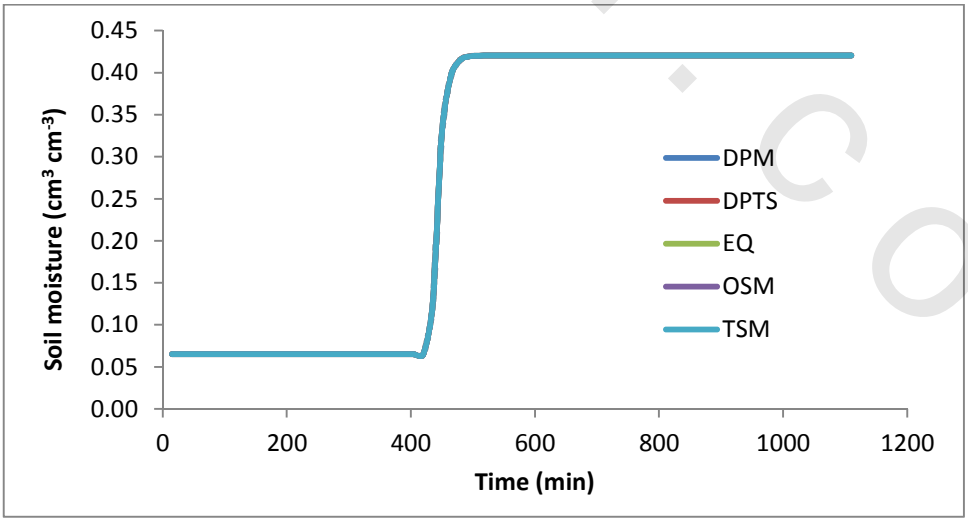

Fig. (20). Soil moisture distribution in soil column of sandy loam soil with medium potassium application at different transport models

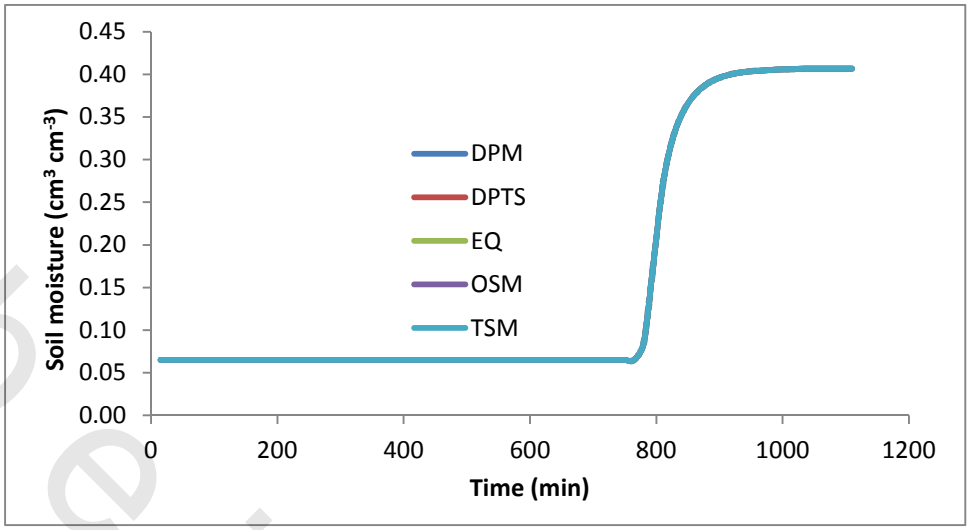

Fig. (21). Soil moisture distribution in soil column of sandy loam soil with high potassium application at different transport models

Figure (22) shows the moisture distribution in sandy loam soil with different K application rates. The figure shows the same trend of moisture distribution that increasing in upper layer and then decreased gradually down to the bottom of soil column. Also, the results show that moisture content of experimental data was more than predicted one. The differences between experimental and predicted data may be due to the soil heterogeneity during packing of soil column under experimental setup.

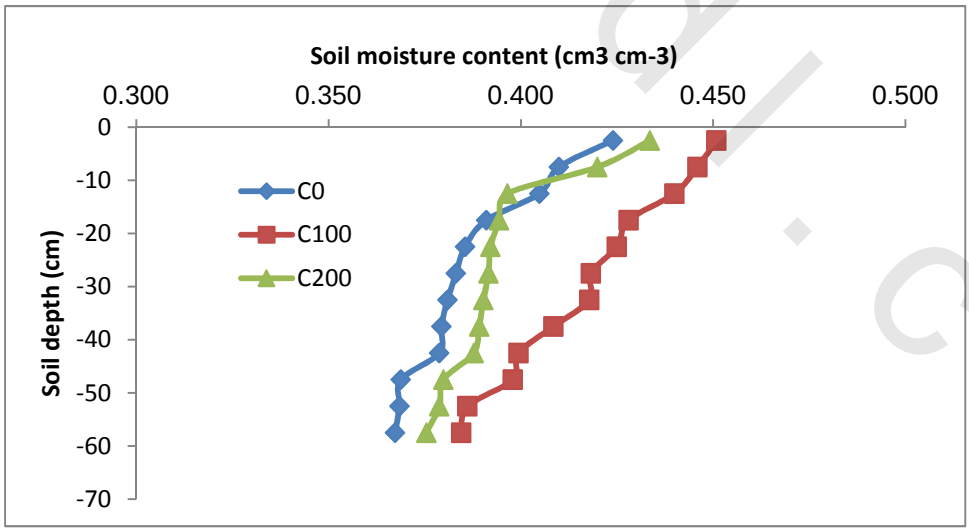

Fig. (22). Soil moisture distribution in soil columns of sandy loam soil with different K application rates (experimental data)

IV.3.1.2. Soluble and sorbed potassium distribution with depth

Figure (23) shows the experimental distribution of potassium concentration through the soil column. The results indicate that potassium was uniformly distributed through the soil profile with low input concentration (12.5 mg/l). While, with medium and high input concentration showed an increase in K concentration in the upper layer (down to 15 cm depth), then the concentration showed the same concentration with high magnitude of high K concentration.

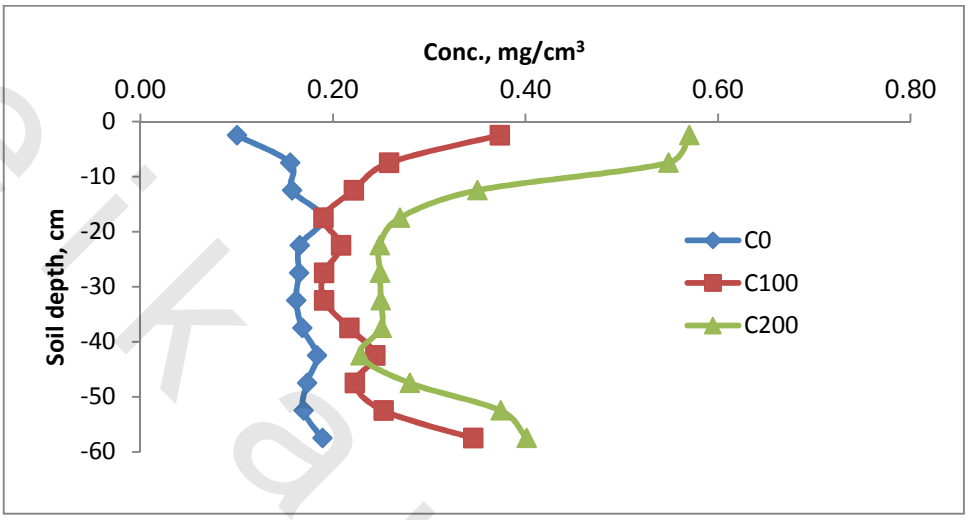

Fig. (23). Potassium distribution with depth for different K input concentration for sandy loam soil (Experimental data)

The K distribution through the soil column was illustrated in Figures (24 to 26) for different equilibrium and non-equilibrium transport models, i.e. equilibrium model (EQ), one-site sorption model (OSM), two-site sorption model (TSM), dual porosity model (DPM) and dual permeability with two-site sorption model (DPTS).

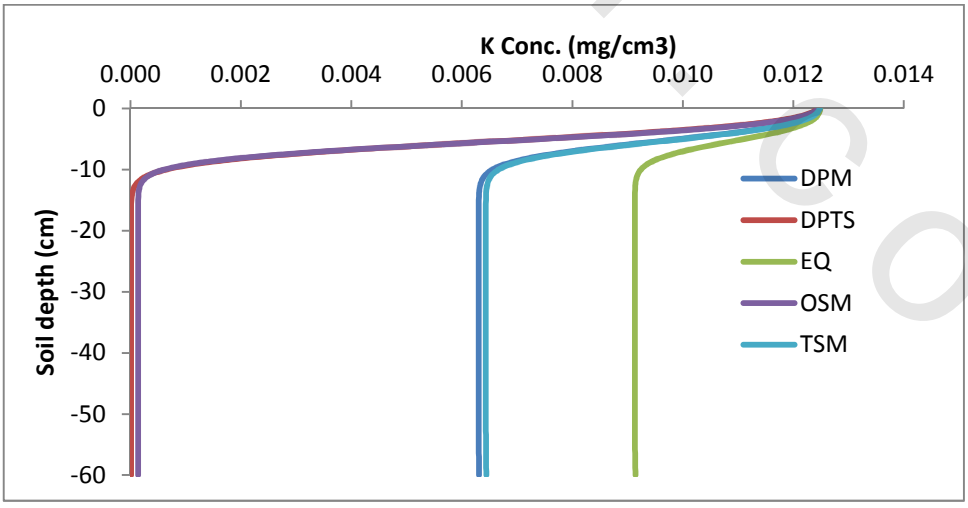

Fig. (24). Potassium distribution with depth for low K input concentration, 12.5 mg/l (modeling data) according to different transport models for sandy loam soil

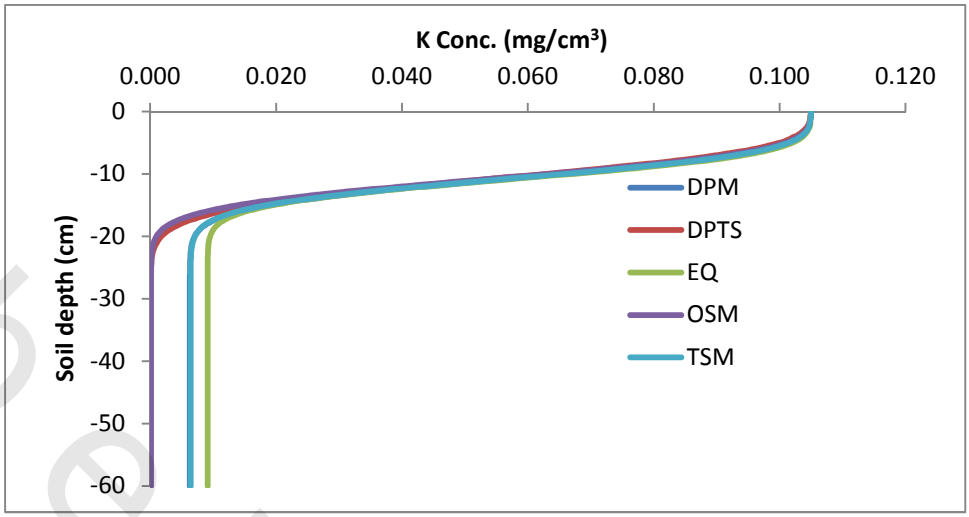

Fig. (25). Potassium distribution with depth for medium K input concentration, 100 mg/l (modeling data) according to different transport models for sandy loam soil

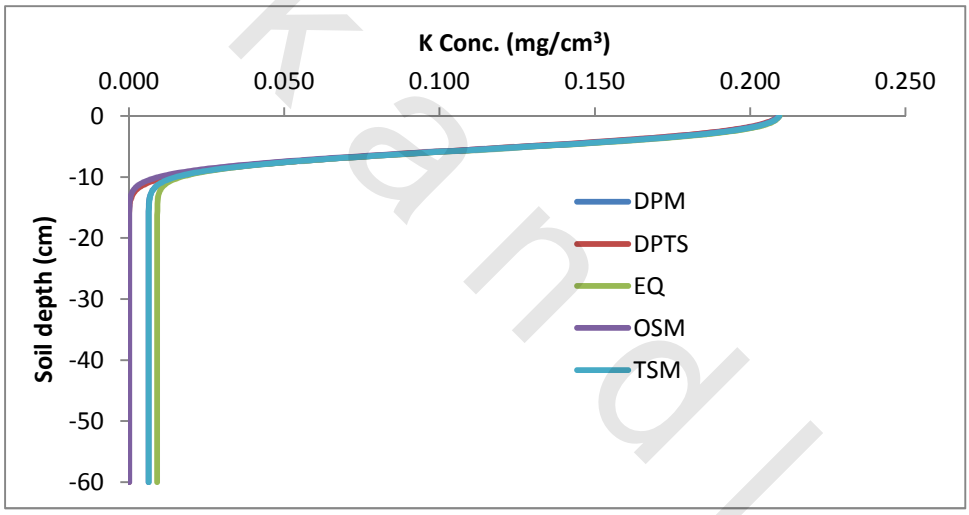

Fig. (26). Potassium distribution with depth for high K input concentration, 200 mg/l (modeling data) according to different transport models for sandy loam soil

The predicted data according to the equilibrium and non-equilibrium transport models showed a symmetrically distribution for medium and high K input concentration. For low K input concentration, the results showed a symmetrically distribution for OSM (one-site sorption model) and DPTS (dual permeability with two-site sorption model). Also, a symmetrically distribution was found with DPM (dual permeability model) and TSM (two –site sorption model). The K distribution of EQ (equilibrium model) has a high values than other four models.

Distribution of sorbed K in soil column according to the equilibrium and non-equilibrium transport models is illustrated in Figures (27 to 29). The modeled data showed that the same trend was found in case of equilibrium model (EQ) at all K input concentration. Also, DPM and TSM were having the same trend and OSM has the higher value of sorbed K in all K input concentrations. The DPTS behave the mid trend of sorbed K. The differences between models may be due to the fraction of exchange sites assumed to be in equilibrium with the liquid phase.

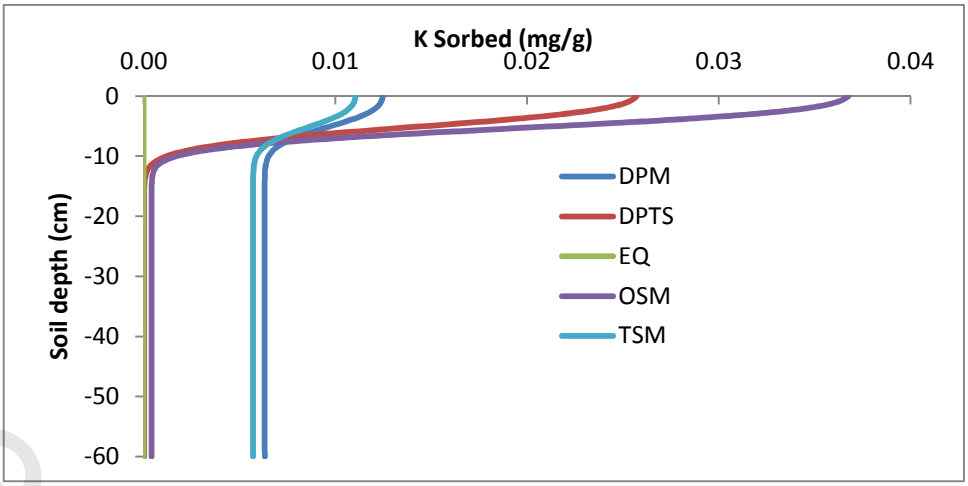

Fig. (27). Distribution of sorbed K on soil matrix for low input concentration (12.5 mg/l) according to different transport models for sandy loam soil

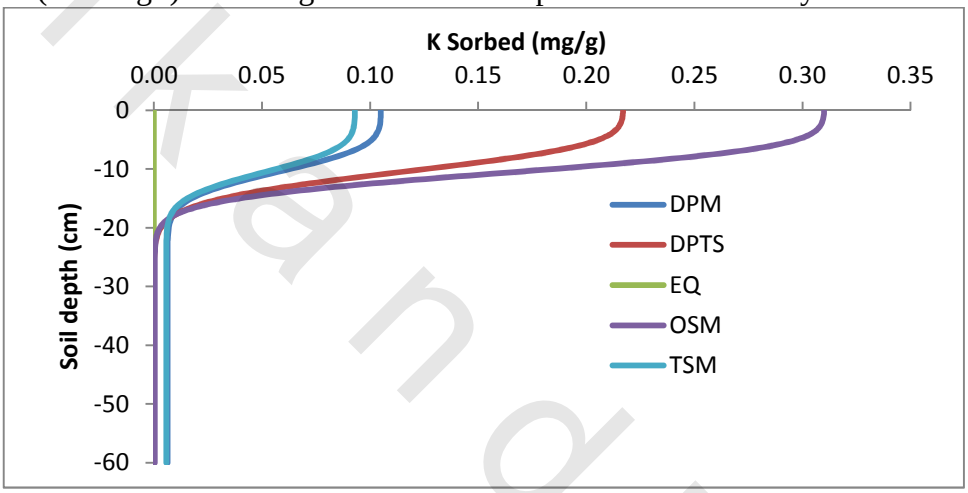

Fig. (28). Distribution of sorbed K on soil matrix for medium input concentration (100 mg/l) according to different transport models for sandy loam soil

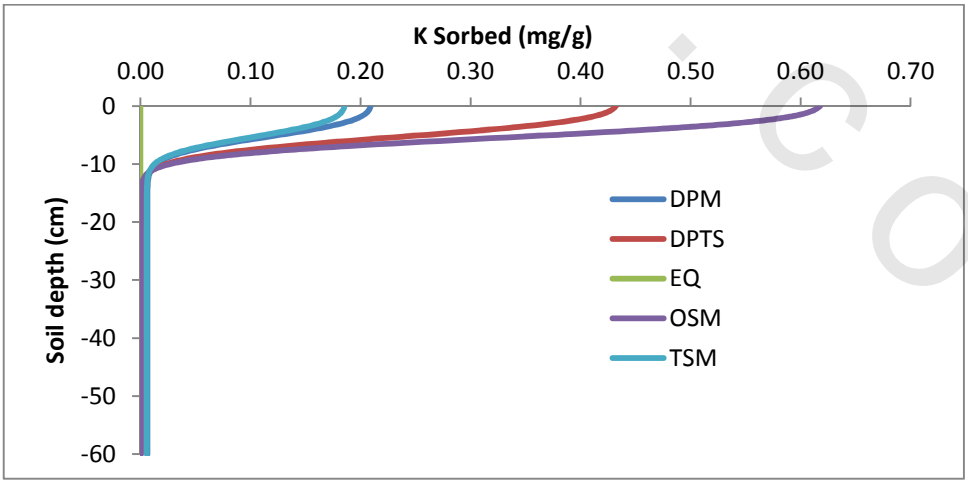

Fig. (29). Distribution of sorbed K on soil matrix for high input concentration (200 mg/l) according to different transport models for sandy loam soil

Figure (30) shows the distribution of sorbed potassium through the soil column according to the experimental data. The results indicate that sorbed potassium was uniformly distributed through the soil profile with medium and high input concentration (100 and 200 mg/l). While, with low input concentration showed a decrease in sorbed K in the upper layer (down to 15 cm depth), then the concentration showed the same trend of medium and high K concentration.

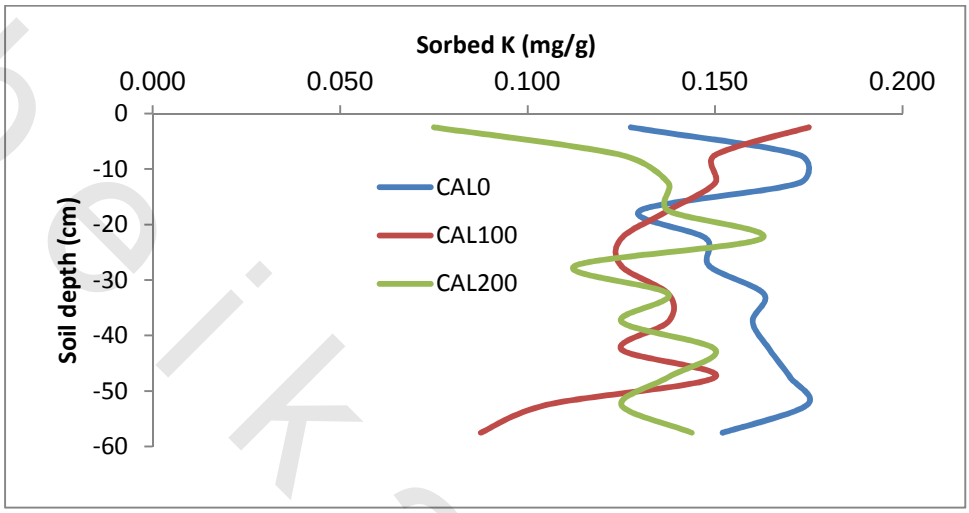

Fig.(30). Sorbed potassium distribution with depth for different K input concentrations (Experimental data) for sandy loam soil

The experimental data show higher values of sorbed and soluble K distribution through the soil column than the modeling data. This result may be due to the soil heterogeneity as results of macropores and preferential flow of water and solute. Preferential flow, as opposed to uniform flow, results in irregular wetting of the soil profile as a direct consequence of water moving faster in certain parts of the soil profile than in others.

IV.3.1.3. Cumulative water flux with time

Figures (31 to 33) show the cumulative water flux with time for sandy loam soil with different transport models. The cumulative water flux shows the uniform trend for all transport models (equilibrium and non-equilibrium models). This result is true because water flux did not dependent on solute concentration but it depends on water flux density that equal for low and high K application rate (0.0233 cm/min), but differed with medium K application rate (0.0454 cm/min).

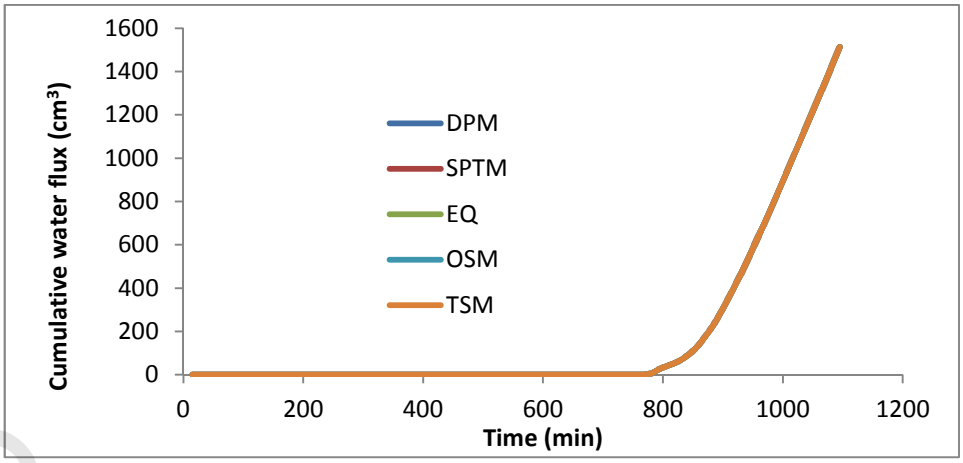

Fig. (31). Cumulative water flux for sandy loam soil at low K application with different transport models

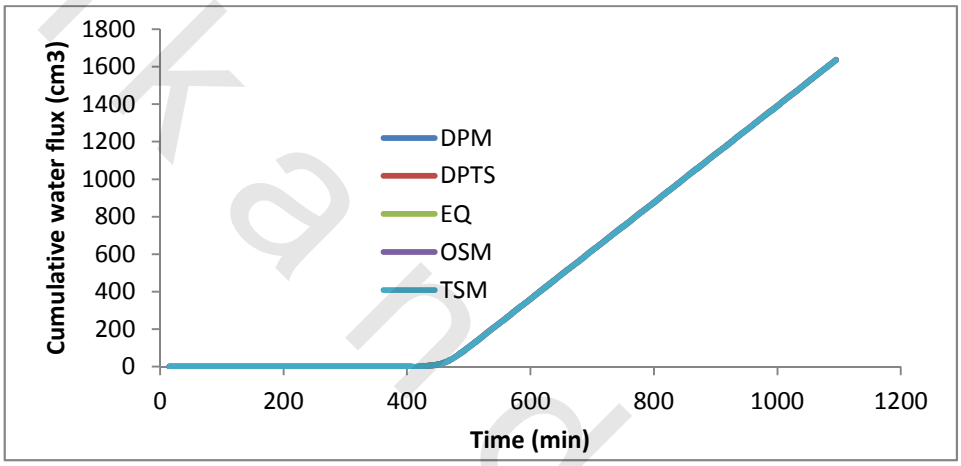

Fig. (32). Cumulative water flux for sandy loam soil at medium K application with different transport models

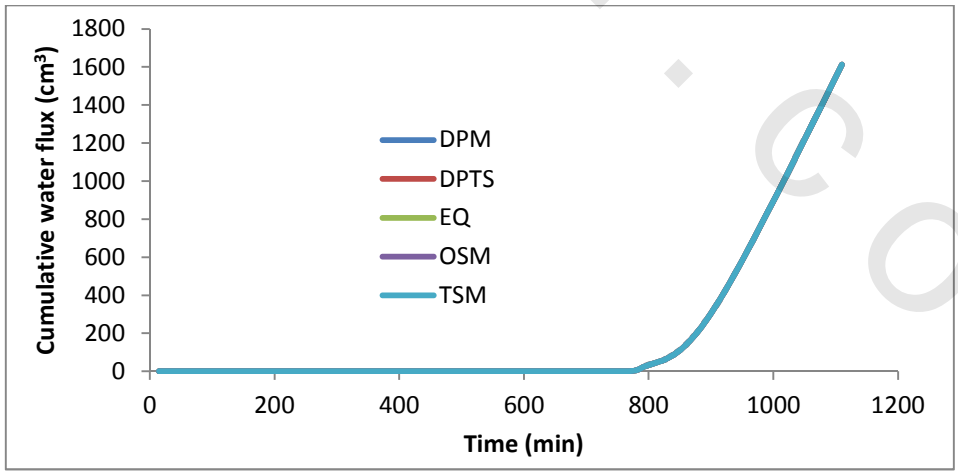

Fig. (33). Cumulative water flux for sandy loam soil at high K application with different transport models

Figure (34) shows the cumulative water flux of medium K input concentration according to the experimental data. The results indicated that cumulative water flux show different values for the K input rates. The high value was recorded for 200 mg/l, while the low value was recorded for control K input. These results did not compatible with model values. The differences may be resulted in the heterogeneity of soil columns such as pore-size distribution, total porosity and may be the packing of soil columns.

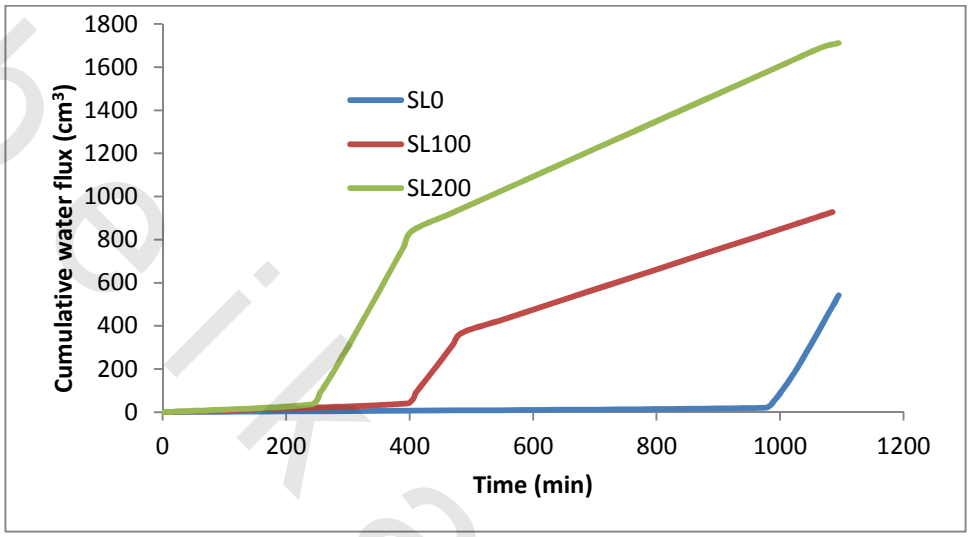

Fig. (34). Cumulative water flux for the sandy loam soil of different K input concentrations (Experimental data)

IV.3.1.4. Cumulative K flux with time

The cumulative K flux with time for sandy loam soil with different transport models is illustrated in Figures (35 to 37). The cumulative K flux differs according to the transport model used for expressing the non-equilibrium transport model. The EQ, DPTS, TSM and OSM transport models have higher K flux out of soil columns in all K application rates.

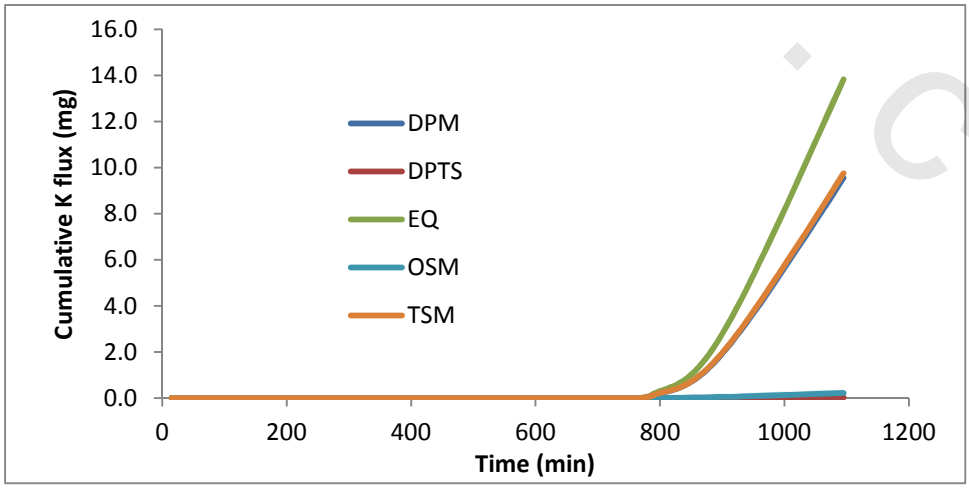

Fig. (35). Cumulative K flux for sandy loam soil column at low K application rate with different transport models

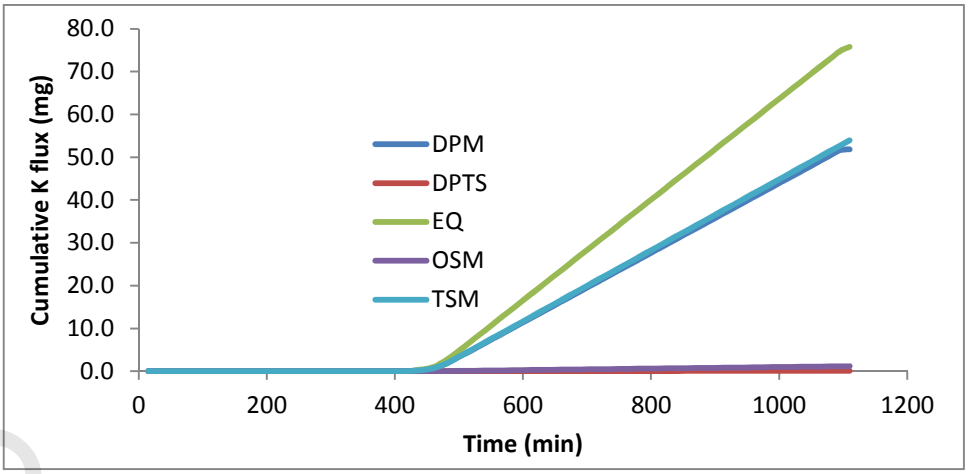

Fig. (36). Cumulative K flux for sandy loam soil column at medium K application rate with different transport models

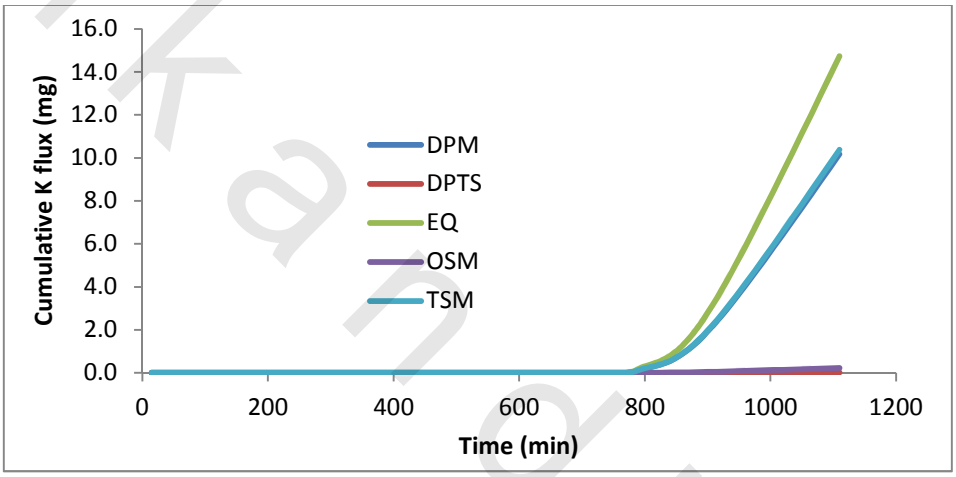

Fig. (37). Cumulative K flux for sandy loam soil column at high K application rate with different transport models

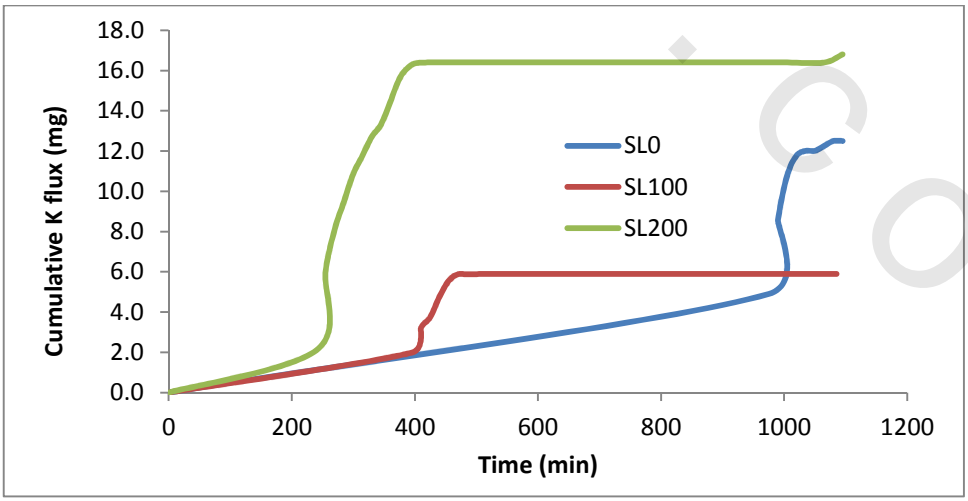

Fig. (38). Cumulative K flux for sandy loam soil of the three K input concentrations (Experimental data)

According to the experimental data (Fig. 38), the results show compatible trend for low and high K input concentrations, but the experiment data did not compatible with modeled data for medium K input concentration.

IV.3.2. Sandy soil

Potassium transport through the sandy soil column was done and applying some equilibrium and non-equilibrium transport models.

IV.3.2.1.Soil moisture distribution

Figures (39 to 41) show the moisture distribution in soil columns of sandy soil with different potassium application. The trend is uniform with all potassium application rates due to about the same rate of solution application as 0.0882 cm/min. All cases reached to the same moisture content (0.361 cm^3 cm^{-3}).

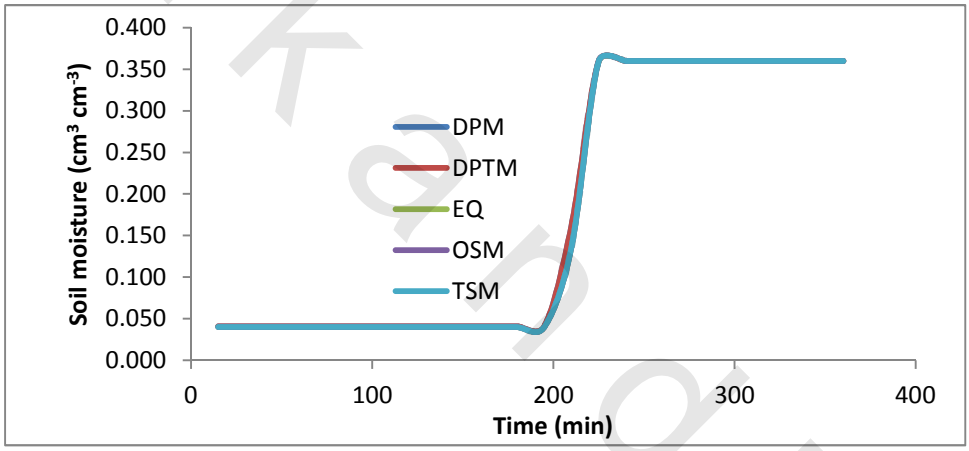

Fig. (39). Soil moisture distribution in soil column of sandy soil with low potassium application at different transport models

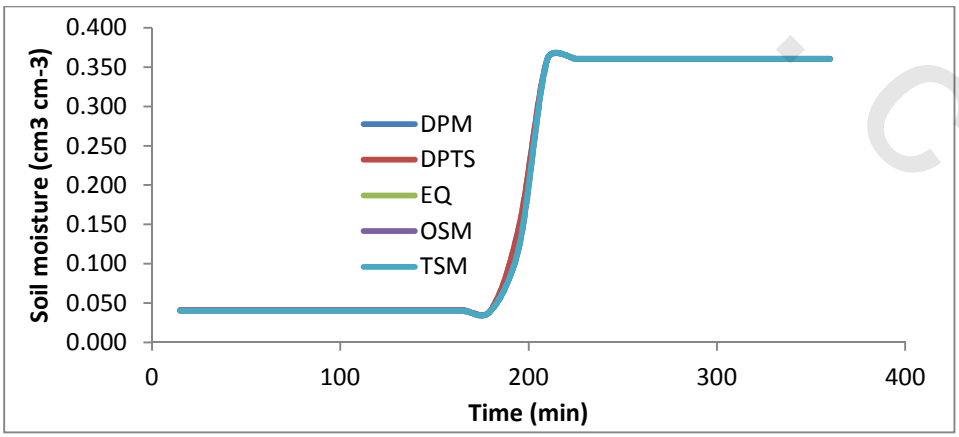

Fig. (40). Soil moisture distribution in soil column of sandy soil with medium potassium application at different transport models

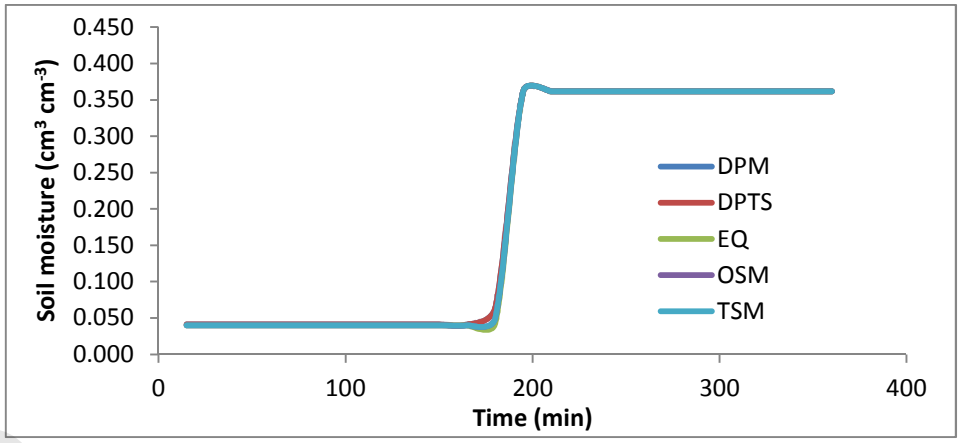

Fig. (41). Soil moisture distribution in soil column of sandy soil with high potassium application at different transport models

Figure (42) shows the moisture distribution in sandy soil with different K application rates. The figure shows the same trend of moisture distribution that increasing in upper layer and then decreased gradually down to the bottom of soil column. Also, the results show that moisture content of experimental data was more than predicted one. The differences between experimental and predicted data may be due to the soil heterogeneity during packing of soil column under experimental setup.

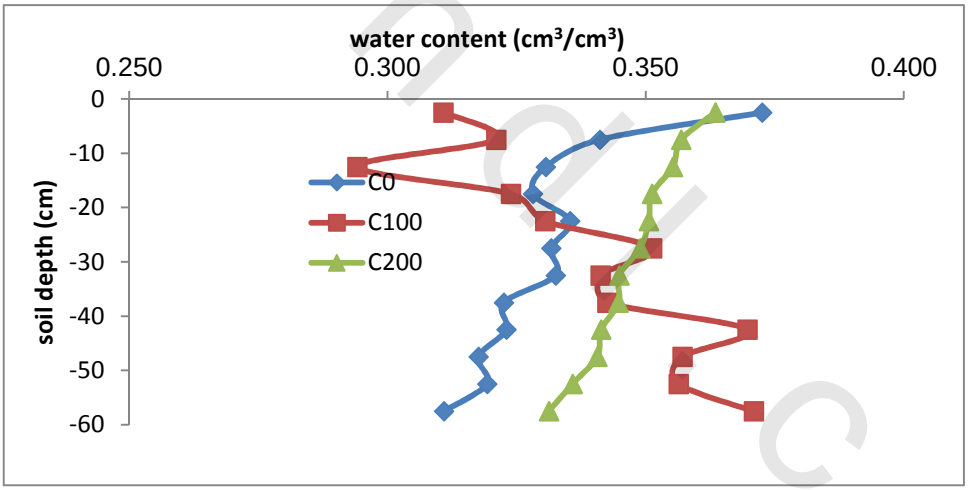

Fig. (42). Soil moisture distribution in soil columns of sandy soil with different K application rates (experimental data)

IV.3.2.2.Soluble potassium distribution with depth

Figure (43) shows the experimental distribution of potassium concentration through the soil column. The results indicate that potassium was uniformly distributed through the soil profile with low input concentration (12.5 mg/l). While, with medium and high input K concentration showed an increase in K concentration in the upper layer (down to 15 cm depth), then the concentration showed the same concentration with medium and high K applications.

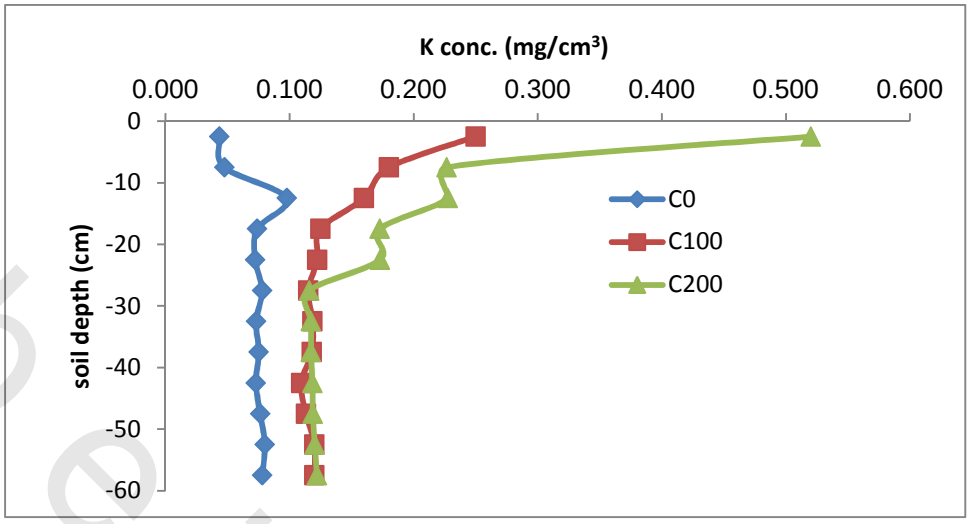

Fig.(43). Potassium distribution with depth for different K input concentration for sandy soil (Experimental data)

The K distribution through the soil column was illustrated in Figures (44 to 46) for different equilibrium and non-equilibrium transport models, i.e. equilibrium model (EQ), one-site sorption model (OSM), two-site sorption model (TSM), dual porosity model (DPM) and dual permeability with two-site sorption model (DPTS).

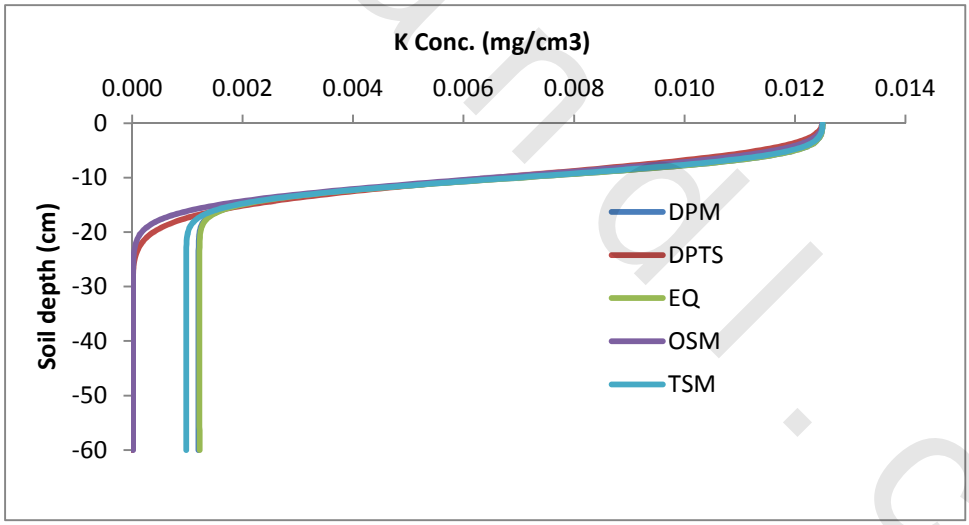

Fig. (44). Potassium distribution with depth for low K input concentration, 12.5 mg/l (modeling data) according to different transport models for sandy soil

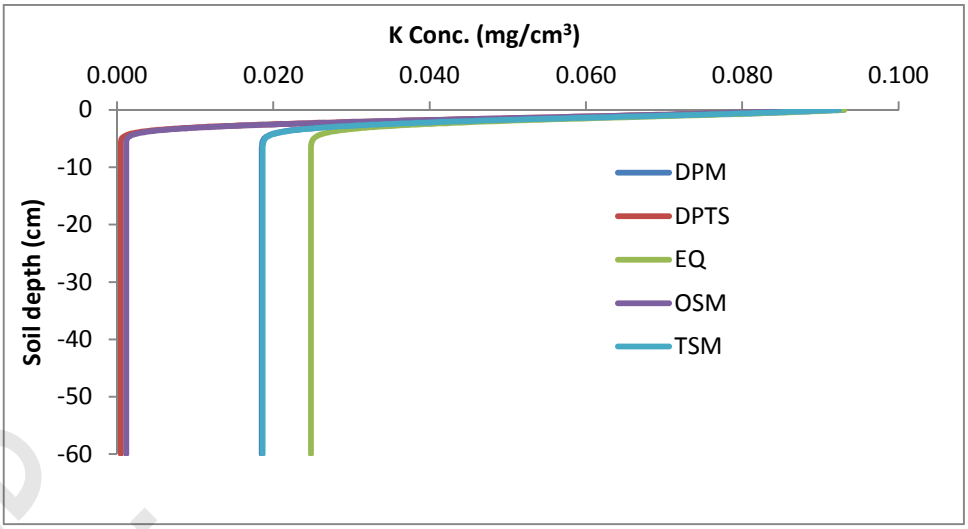

Fig. (45). Potassium distribution with depth for medium K input concentration, 100 mg/l (modeling data) according to different transport models for sandy soil

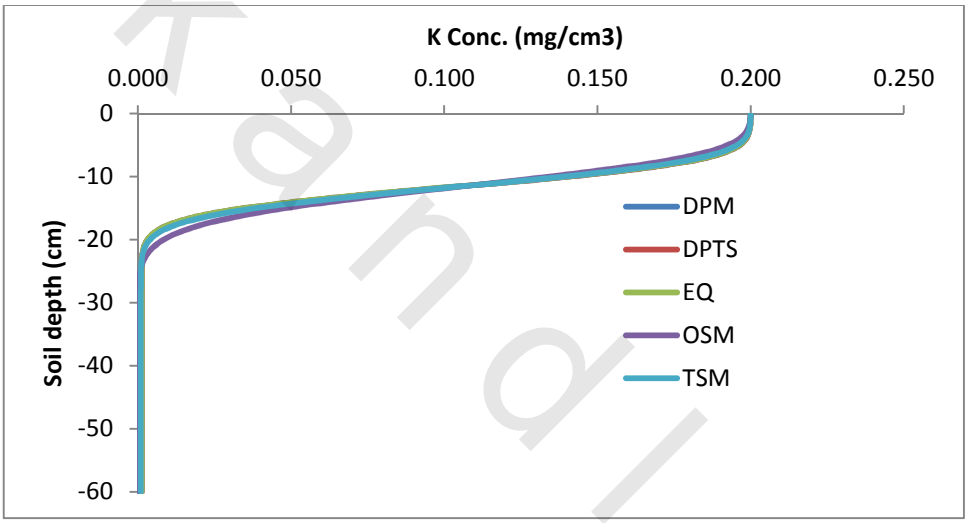

Fig. (46). Potassium distribution with depth for high K input concentration, 200 mg/l (modeling data) according to different transport models for sandy soil

The predicted data according to the equilibrium and non-equilibrium transport models showed a symmetrically distribution for low and high K input concentration. For medium K input concentration, the results showed a symmetrically distribution for EQ (Equilibrium model) and TSM (two-site sorption model). Also, a symmetrically distribution was found with DPTS (dual permeability with two site model) and DPM (dual porosity model). The K distribution of EQ (equilibrium model) has a high values than other models.

Distribution of sorbed K on soil columns according to the equilibrium and non-equilibrium transport models is illustrated in Figures (47 to 49). The predicted data showed that the same trend was found in case of OSM, DPTS, TSM non-equilibrium models at all K input concentration. The differences between models may be due to the fraction of exchange sites assumed to be in equilibrium with the liquid phase.

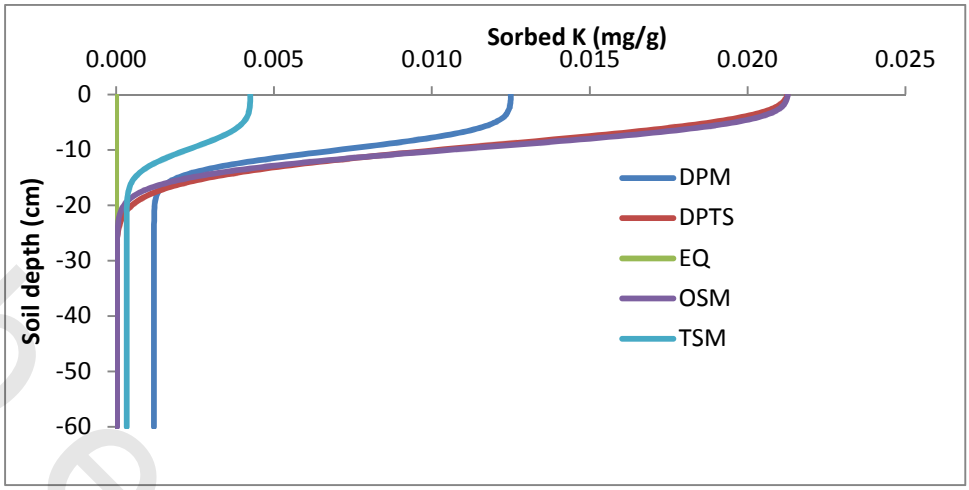

Fig. (47). Distribution of sorbed K on soil matrix for low input concentration (12.5 mg/l) according to different transport models for sandy soil

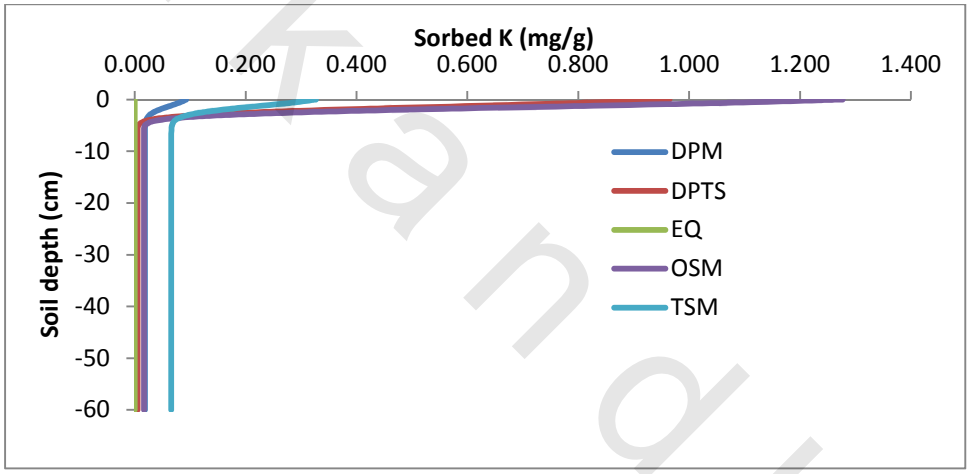

Fig. (48). Distribution of sorbed K on soil matrix for medium input concentration (100 mg/l) according to different transport models for sandy soil

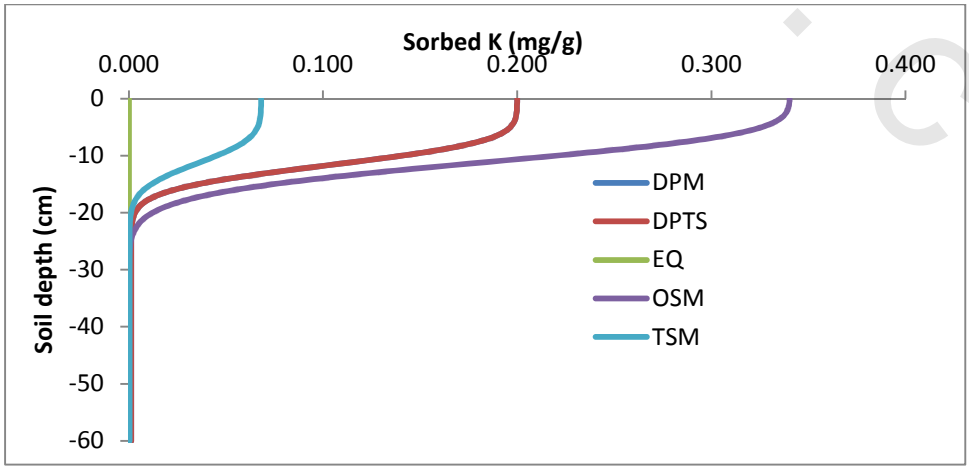

Fig. (49). Distribution of sorbed K on soil matrix for high input concentration (200 mg/l) according to different transport models for sandy soil

Figure (50) shows the distribution of sorbed potassium through the soil column according to the experimental data. The results indicate that sorbed potassium was uniformly distributed through the soil profile with low input concentration (12.5 mg/l). While, with medium and high input concentration showed an increase in sorbed K in the upper layer (down to 15 cm depth), then the concentration showed the same trend.

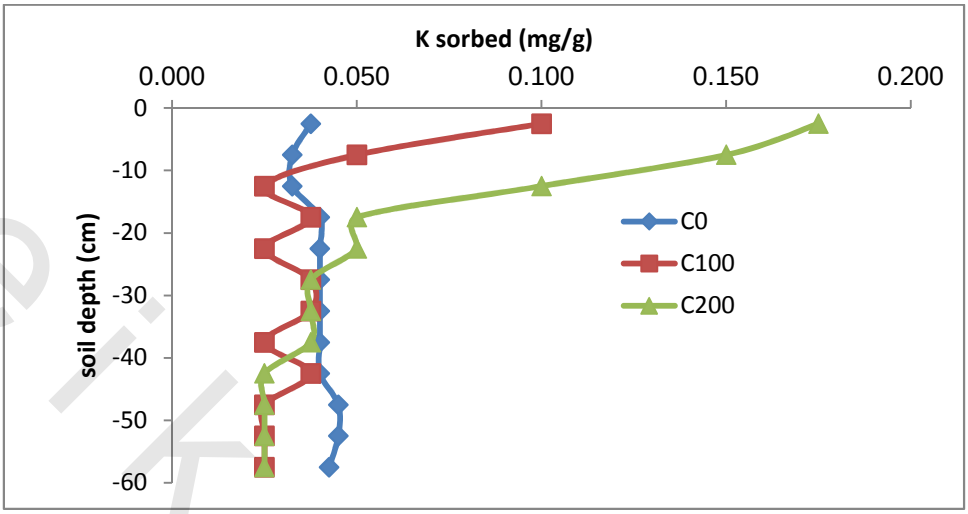

Fig.(50). Sorbed potassium distribution with depth for different K input concentrations for sandy soil (Experimental data)

The experimental data show higher values of sorbed and soluble K distribution through the soil profile than the modeling data. This result may be due to the soil heterogeneity as results of macropores and preferential flow of water and solute. Preferential flow, as opposed to uniform flow, results in irregular wetting of the soil profile as a direct consequence of water moving faster in certain parts of the soil profile than in others.

IV.3.2.3.Cumulative water flux with time

Figures (51 to 53) show the cumulative water flux with time for sandy soil with different transport models. The cumulative water flux shows the uniform trend for all transport models (equilibrium and non-equilibrium models). This result is true because water flux did not depend on solute concentration but it depends on water flux density that equal for all K application rate.

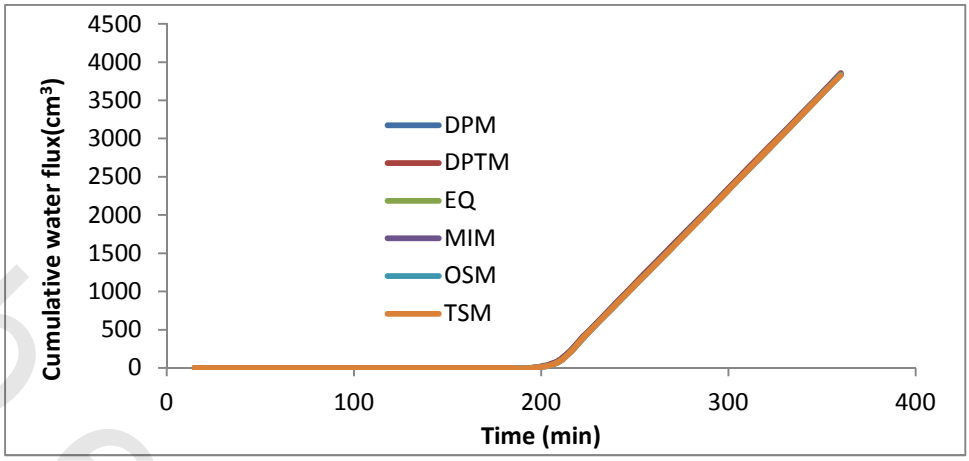

Fig. (51). Cumulative water flux for sandy soil at low K application with different transport models

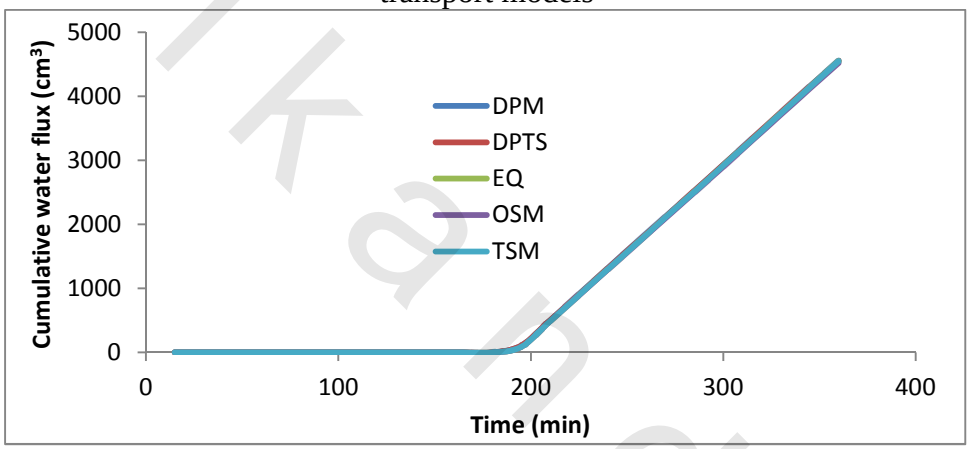

Fig. (52). Cumulative water flux for sandy soil at medium K application with different transport models

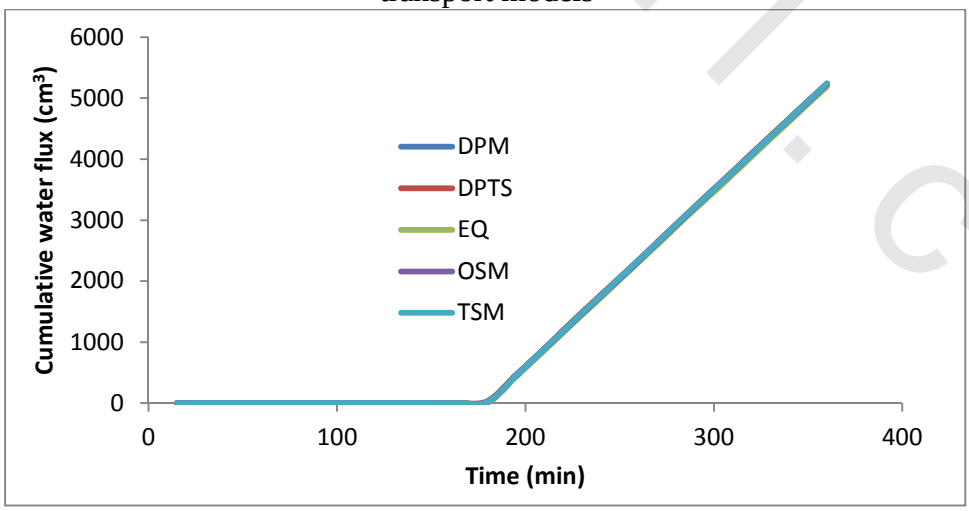

Fig. (53). Cumulative water flux for sandy soil at high K application with different transport models

The experimental data show about the same trend of the cumulative flux through the soil profile sandy soil, the values were not compatible with modeled data. This result may be due to the soil heterogeneity as results of macropores, preferential flow of water and pore-size distribution during soil packing. Preferential flow, as opposed to uniform flow, results in irregular wetting of the soil profile as a direct consequence of water moving faster in certain parts of the soil profile than in others (Fig. 54).

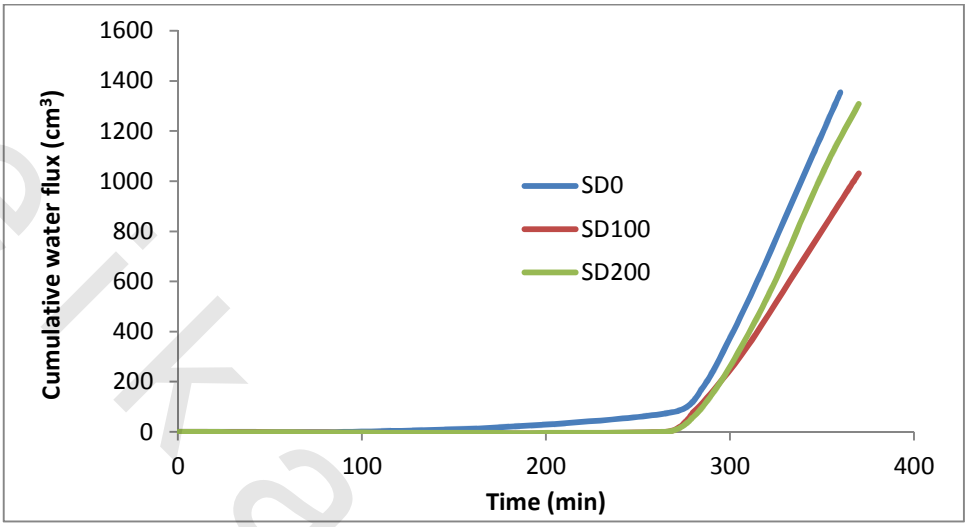

Fig. (54). Cumulative water flux for sandy soil for K application concentration (experimental data)

IV.3.2.4. Cumulative K flux with time

The cumulative K flux with time for sandy soil with different transport models is illustrated in Figures (55 to 57). The cumulative K flux differs according to the transport models used for expressing the non-equilibrium transport condition. The EQ and TSM transport models have higher K flux out of soil columns in all K application rates.

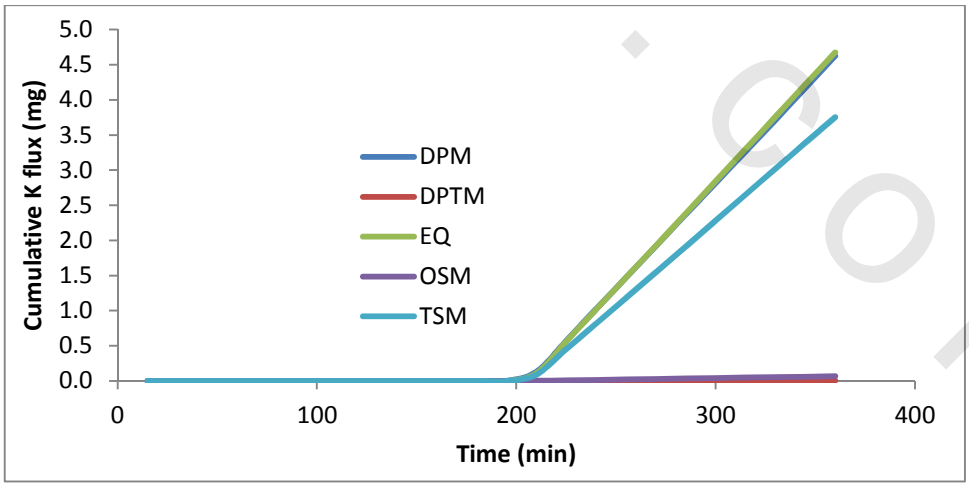

Fig. (55). Cumulative K flux for sandy soil column at low K application rate with different transport models

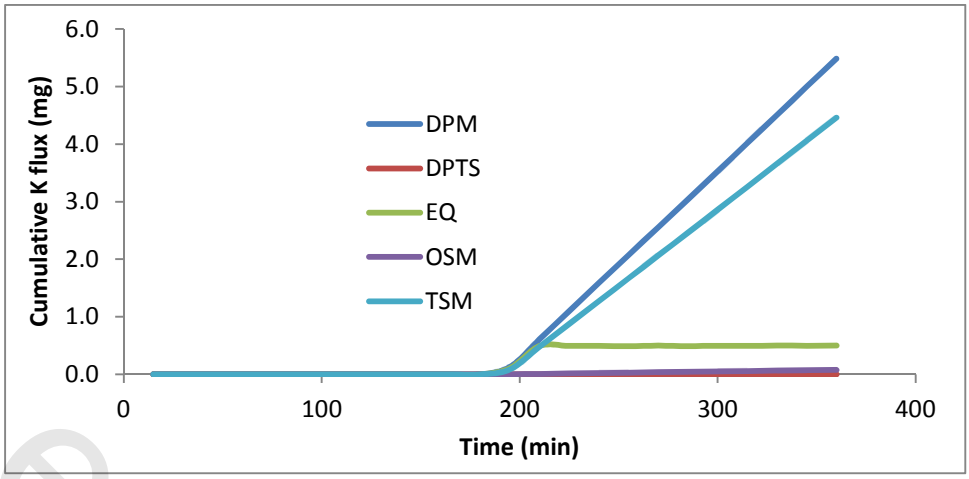

Fig. (56). Cumulative K flux for sandy soil column at medium K application rate with different transport models

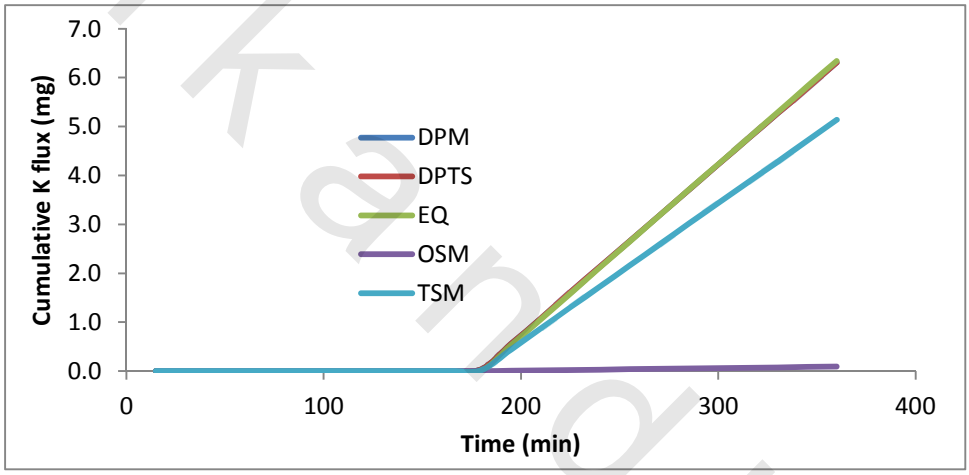

Fig. (57). Cumulative K flux for sandy soil column at high K application rate with different transport models

Figure (58) shows the experimental distribution of cumulative K flux through the sandy soil columns under different K input concentration. The results show about the same trend in case of control and 100 mg/l K input, but for 200 mg/l K input, the experimental data illustrate higher values than model data. The differences between the experimental and model data may be referred to the heterogeneity of soil columns according to pore-size distribution and macropores heterogeneity.

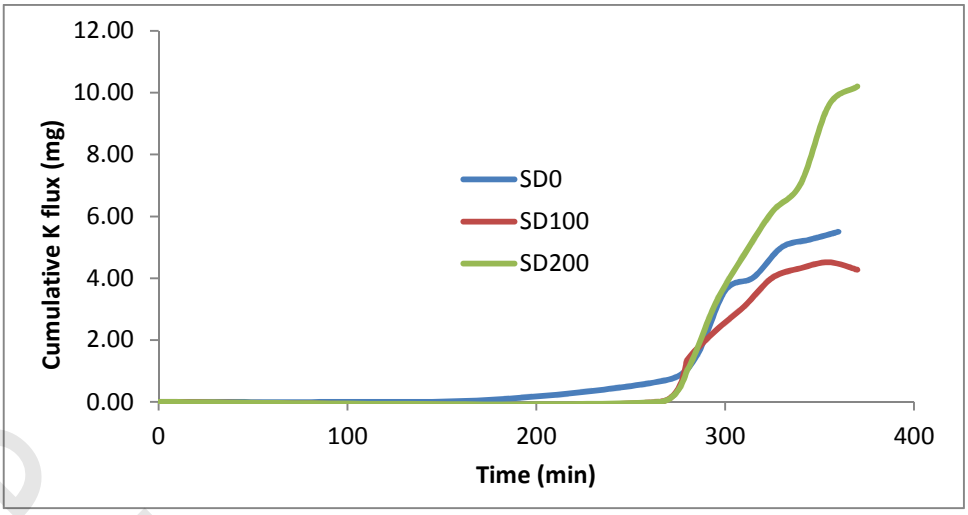

Fig. (58). Cumulative K flux for sandy soil of K input concentrations (Experimental data)

IV.3.3. Sandy clay loam soil

Potassium transport through the sandy clay loam soil columns was done , applying some equilibrium and non-equilibrium transport models.

IV.3.3.1. Soil moisture distribution

Figures (59 to 61) show the moisture distribution in soil columns of sandy clay loam soil with different potassium application. The trend is uniform with all potassium application rates, but there is some differences between the three cases according to the water flux rate and time of application.

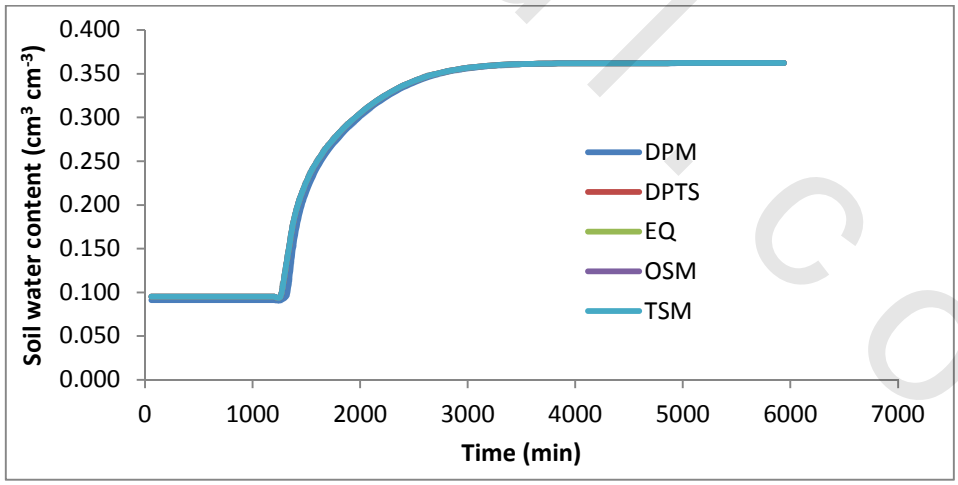

Fig. (59). Soil moisture distribution in soil column of sandy clay loam soil with low potassium application at different transport models

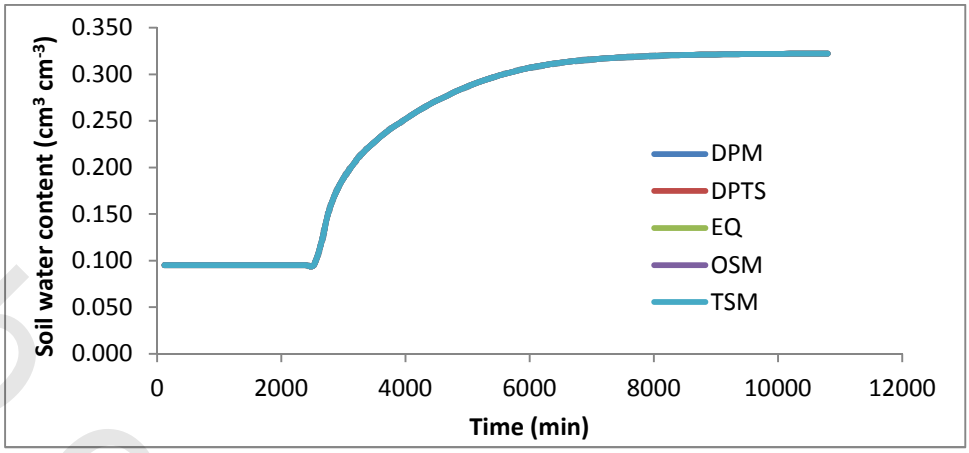

Fig. (60). Soil moisture distribution in soil column of sandy clay loam soil with medium potassium application at different transport models

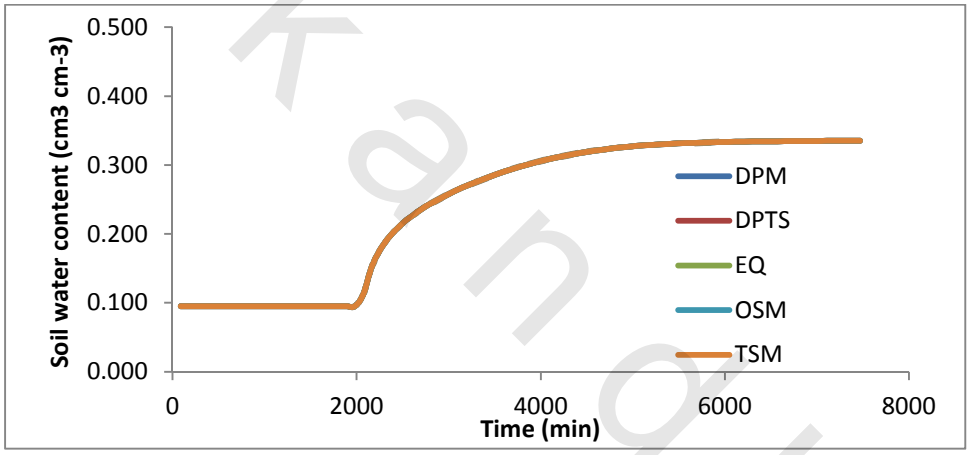

Fig. (61). Soil moisture distribution in soil column of sandy clay loam soil with high potassium application at different transport models

Figure (62) shows the moisture distribution in sandy clay loam soil with different K application rates. The figure shows the same trend of moisture distribution that increasing in upper layer and then decreased gradually down to the bottom of soil column. Also, the results show that moisture content of experimental data was more than predicted one. The differences between experimental and predicted data may be due to the soil heterogeneity during packing of soil column under experimental setup.

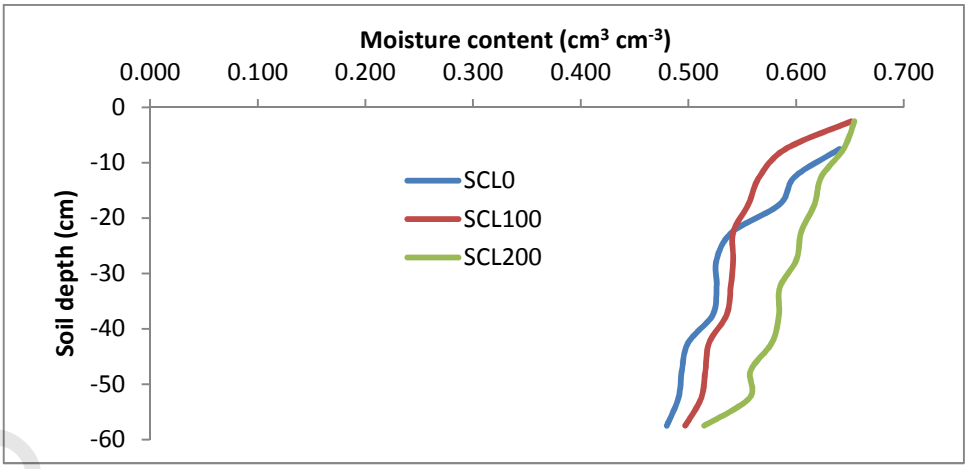

Fig. (62). Soil moisture distribution in soil columns of sandy clay loam soil with different K application rates (experimental data)

IV.3.3.2. Soluble and sorbed potassium distribution with depth

Figure (63) shows the distribution of potassium concentration through the soil column. The results indicate that potassium was uniformly distributed through the soil profile with low input concentration (12.5 mg/l). While, with medium and high input K concentration showed an increase in K concentration in the upper layer (down to 15 cm depth), then the concentration showed the same concentration with medium and high K applications.

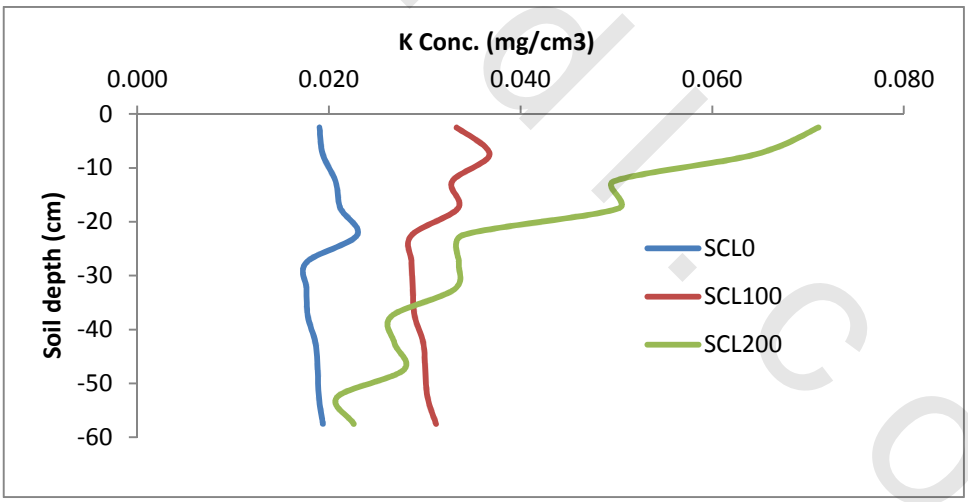

Fig. (63). Potassium distribution with depth for different K input concentration for sandy clay loam soil (Experimental data)

The K distribution through the soil column of sandy clay loam soil was illustrated in Figures (64 to 66) for different equilibrium and non-equilibrium transport models, i.e. equilibrium model (EQ), one-site sorption model (OSM), two-site sorption model (TSM), dual porosity model (DPM) and dual permeability with two-site sorption model (DPTS).

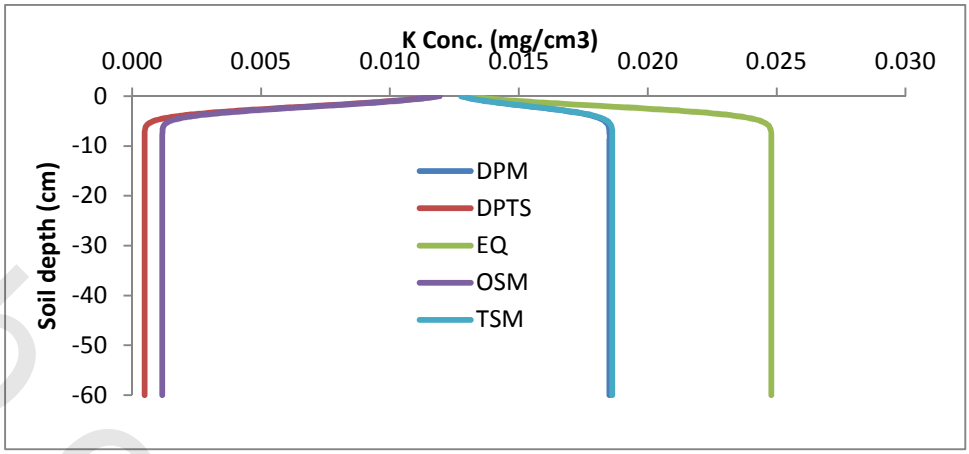

Fig. (64). Potassium distribution with depth for low K input concentration, 12.5 mg/l (modeling data) according to different transport models for sandy clay loam soil

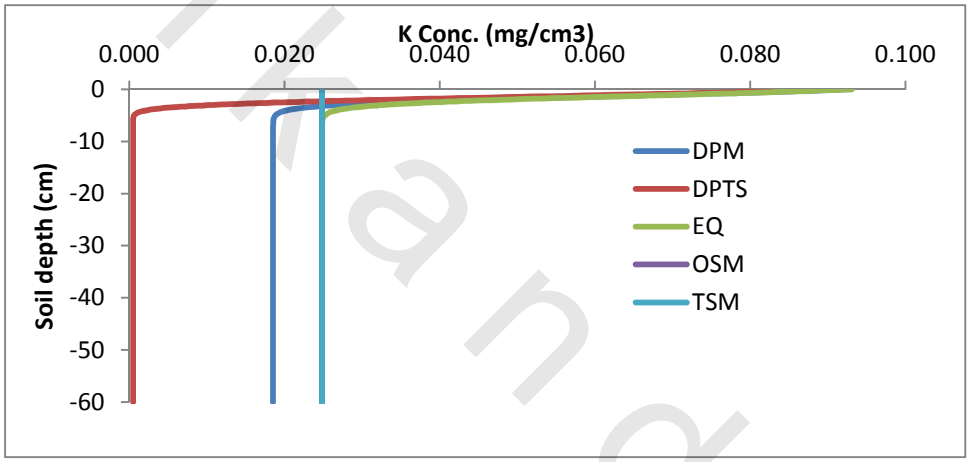

Fig. (65). Potassium distribution with depth for medium K input concentration,100 mg/l (modeling data) according to different transport models for sandy clay loam soil

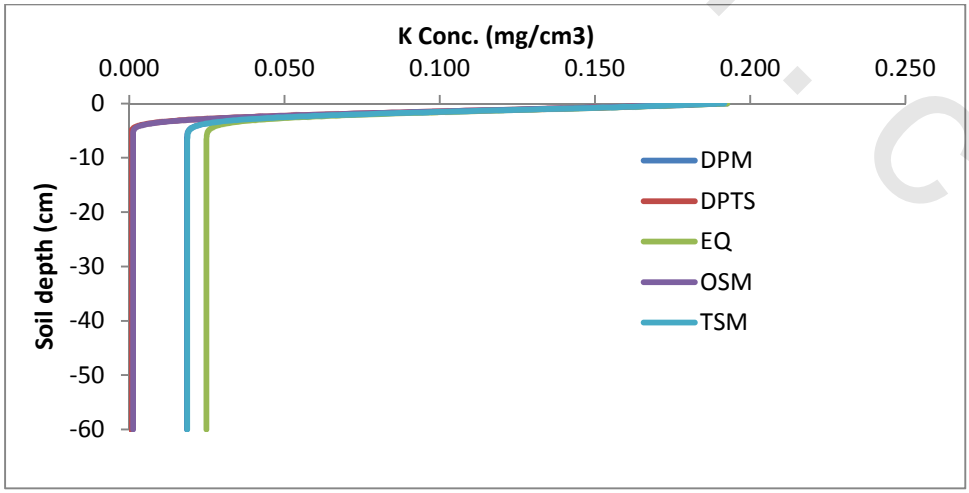

Fig. (66). Potassium distribution with depth for high K input concentration, 200 mg/l (modeling data) according to different transport models for sandy clay loam soil

The predicted data according to the equilibrium and non-equilibrium transport models showed a symmetrically distribution for medium and high K input concentration. For low K input concentration, the results showed a symmetrically distribution for all transport models down to 5 cm depth with high values of EQ and DPM.

Distribution of sorbed K on soil columns according to the equilibrium and non-equilibrium transport models is illustrated in Figures (67 to 69). The predicted data showed that the same trend was found in case of OSM, DPTS, TSM non-equilibrium models at all K input concentrations down to 5 cm soil depth. The differences between models may be due to the fraction of exchange sites assumed to be in equilibrium with the liquid phase.

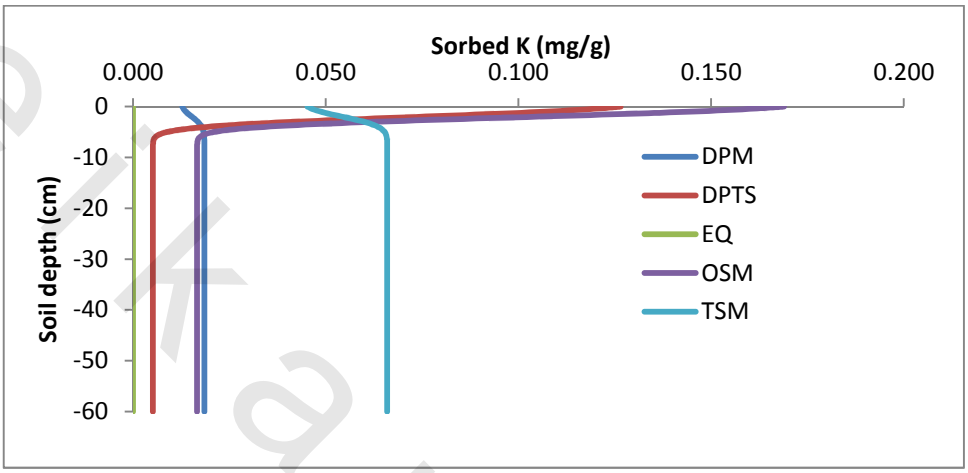

Fig. (67). Distribution of sorbed K on soil matrix for low input concentration (12.5 mg/l) according to different transport models for sandy clay loam soil

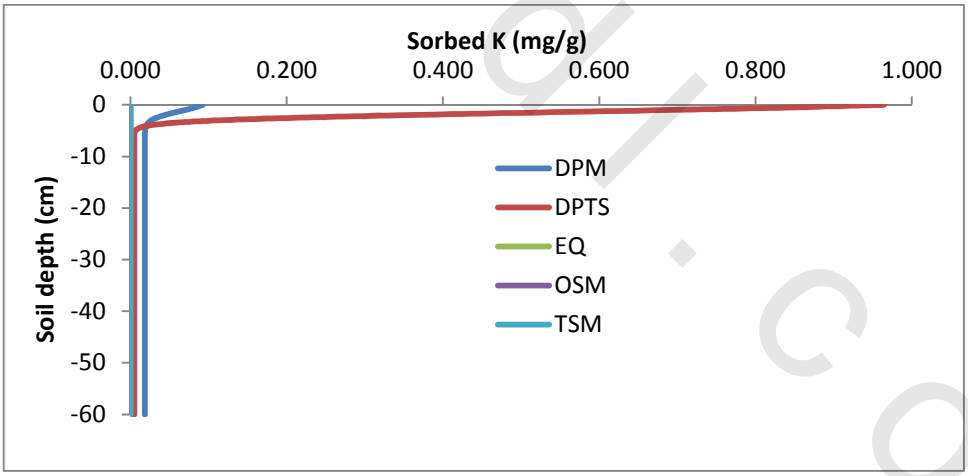

Fig. (68). Distribution of sorbed K on soil matrix for medium input concentration (100 mg/l) according to different transport models for sandy clay loam soil

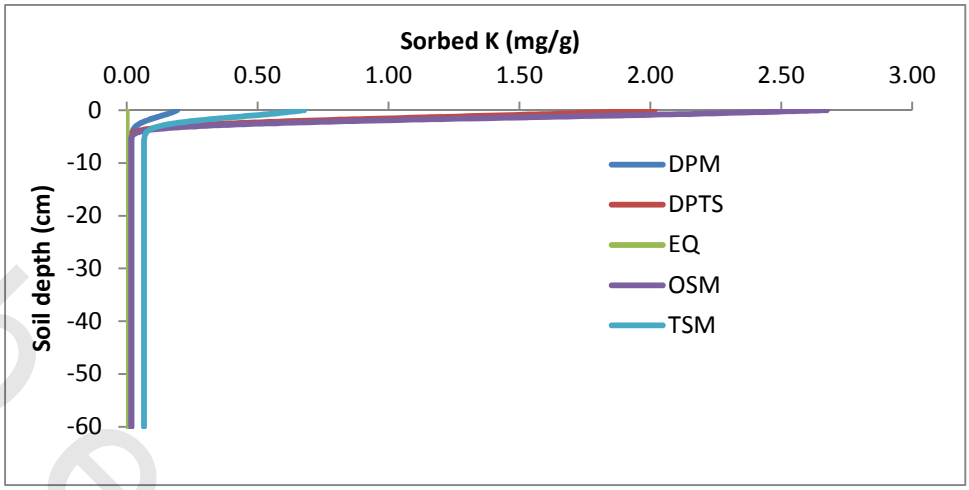

Fig. (69). Distribution of sorbed K on soil matrix for high input concentration (200 mg/l) according to different transport models for sandy clay loam soil

Figure (70) shows the distribution of sorbed potassium through the soil column according to the experimental data. The results indicate that sorbed potassium was uniformly distributed through the soil profile with all input concentrations. The same trend with different magnitude was observed for all K input except the medium K input is higher in the surface layer down to 5 cm.

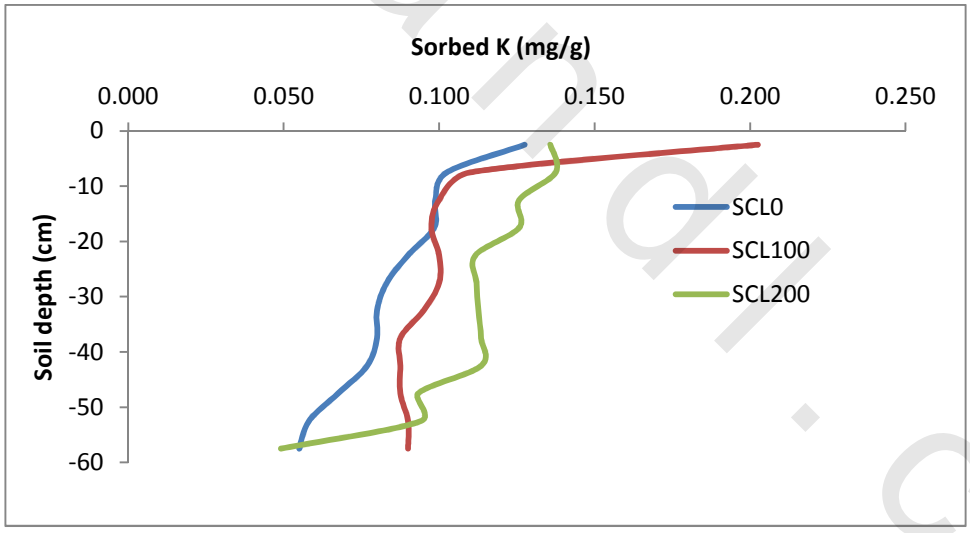

Fig. (70). Sorbed potassium distribution with depth for different K input concentrations for sandy clay loam soil (Experimental data)

The experimental data show higher values of sorbed and soluble K distribution through the soil profile than the modeling data. This result may be due to the soil heterogeneity as results of macropores and preferential flow of water and solute. Preferential flow, as opposed to uniform flow, results in irregular wetting of the soil profile as a direct consequence of water moving faster in certain parts of the soil profile than in others.

IV.3.3.3.Cumulative water flux with time

Figures (71 to 73) show the cumulative water flux with time for sandy soil with different transport models. The cumulative water flux shows the uniform trend for all transport models (equilibrium and non-equilibrium models). This result is true because water flux did not depend on solute concentration but it depends on water flux density that differed in the treatments (water application time).

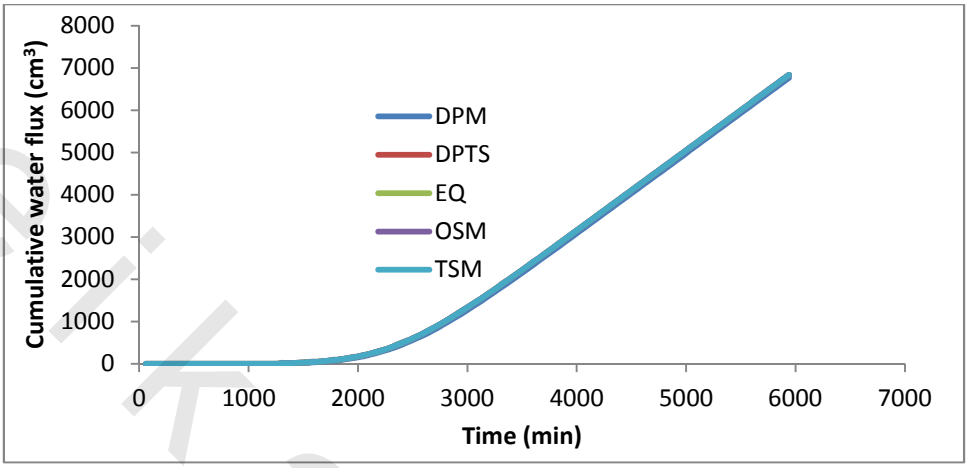

Fig. (71). Cumulative water flux for sandy clay loam soil at low K application with different transport models

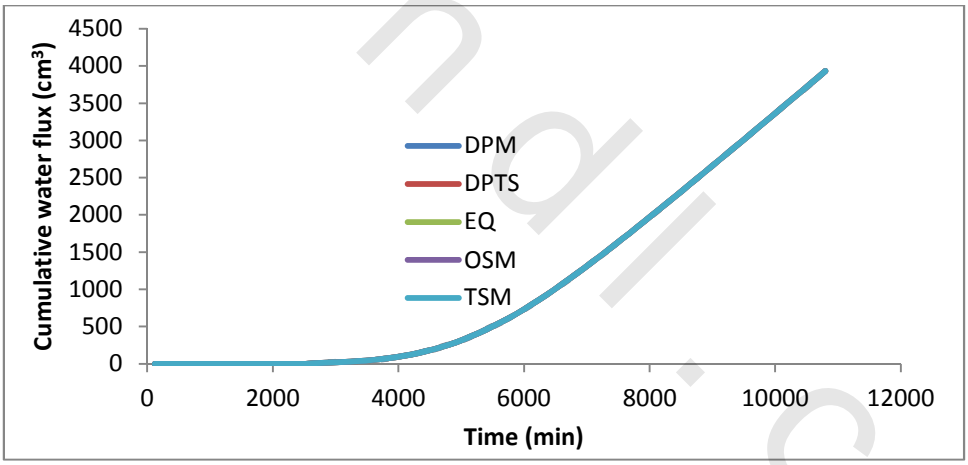

Fig. (72). Cumulative water flux for sandy clay loam soil at medium K application with different transport models

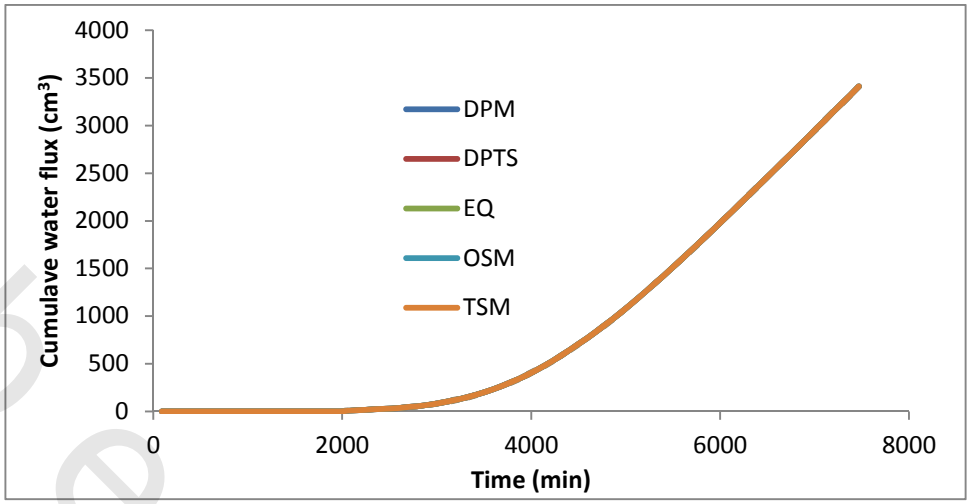

Fig. (73). Cumulative water flux for sandy clay loam soil at high K application with different transport models

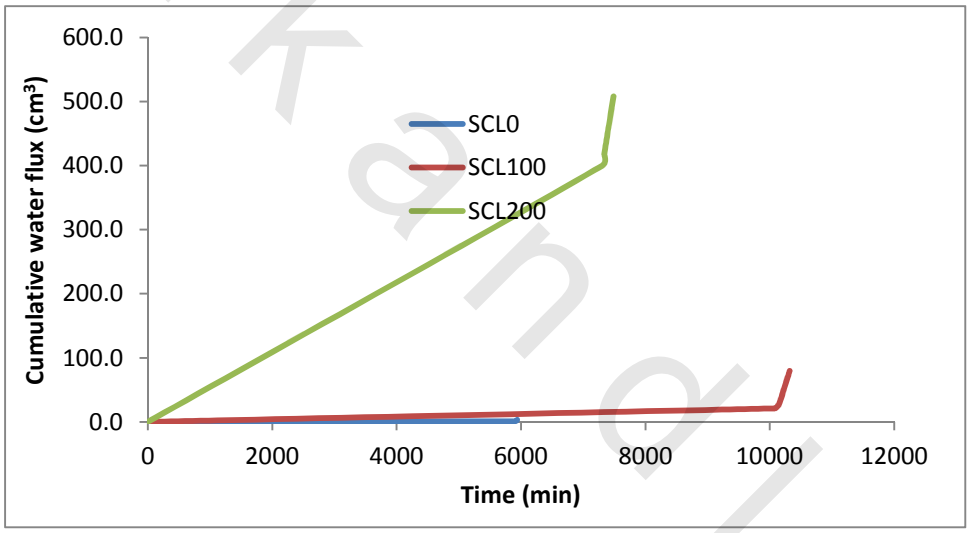

Fig. (74). The experimental data of cumulative water flux for sandy clay loam soil at the three K applications

IV.3.3.4.Cumulative K flux with time

The cumulative K flux with time for sandy soil with different transport models is illustrated in Figures (75 to 77). The cumulative K flux differs according to the transport models used for expressing the non-equilibrium transport condition. The EQ, DPM and TSM transport models have higher K flux out of soil columns at all K application rates.

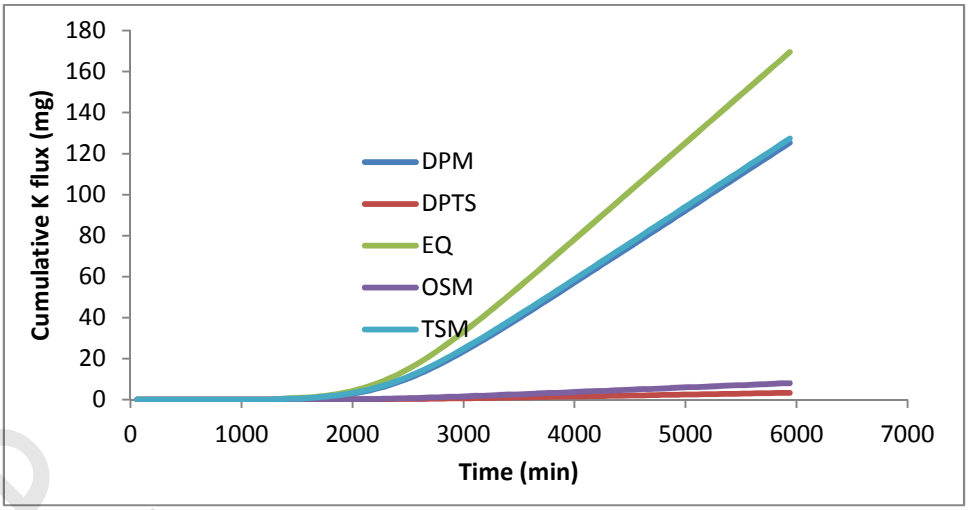

Fig. (75). Cumulative K flux for sandy clay loam soil column at low K application rate with different transport models

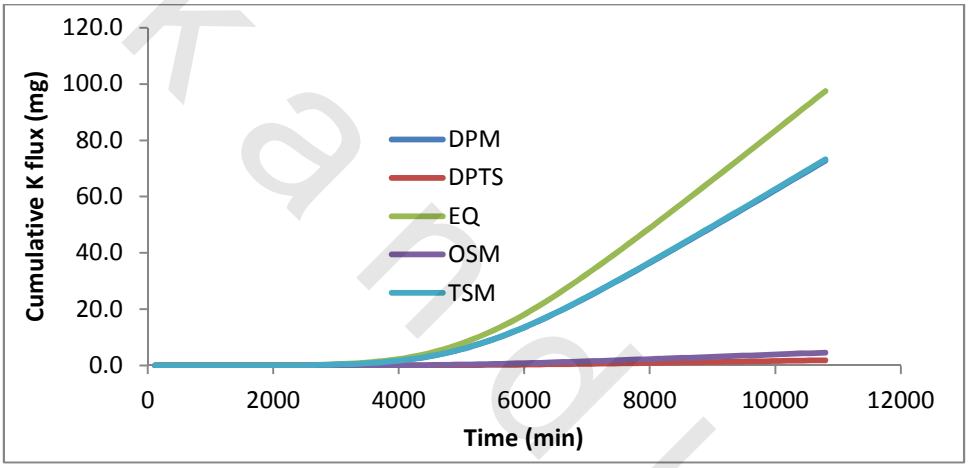

Fig. (76). Cumulative K flux for sandy clay loam soil column at medium K application rate with different transport models

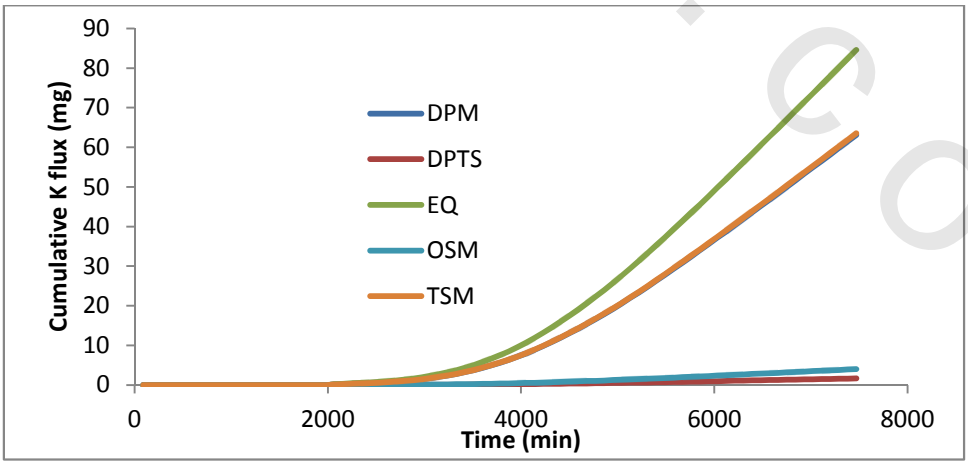

Fig. (77). Cumulative K flux for sandy clay loam soil column at high K application rate with different transport models

Figure (78) shows the experimental data of cumulative K flux through sandy clay loam soil columns at different K input concentrations. The results did not compatible with model data. The obtained results may be due to the macropores or preferential flow according the pore-size distribution.

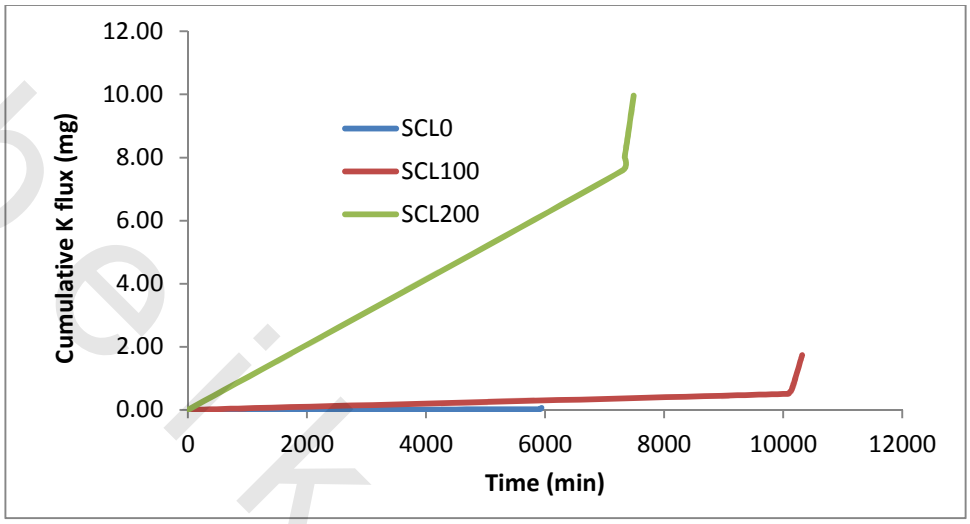

Fig. (78). The experimental data of cumulative K flux for sandy clay loam soil at the three K applications

The obtained results of the present study show that there are differences between experimental and predicted data according to HYDRUS-1D. The non-equilibrium simulation of potassium transport in the three soil textures did not fully represent the experimental data. These differences may be due to the heterogeneity of soil packing and also due to the macropores flow phenomena. Soil heterogeneity is responsible for the difficulty in predicting the movement of mass (solids, liquids and gases) in field situations at most scales. For example, it often results in faster movement of gas, water, solutes and particles than would be expected from the soil matrix properties. This more rapid mass transport is associated with processes such as flow through earthworm burrows, cracks in soil, or flow associated with soil layering and hydrophobicity. These processes, together, are called preferential flow (PF). Preferential flow (PF): refers to flow mechanisms where transport of water together with dissolved or suspended matter is primarily associated with a smaller fraction of the total pore network, at any scale much larger than the microscopic.

Two types of soil heterogeneity which require different modelling approaches are distinguished: micro- and macro-heterogeneity. **Micro-heterogeneity** refers to the heterogeneity at the pore scale due to the presence of macropores which form a separate pore network and **macro-heterogeneity** refers to the spatial variability of macroscopic soil properties which define flow and transport at a macroscopic scale. Water flow and solute transport in natural soils are significantly influenced by the occurrence of (1) macropores and structured elements (micro-heterogeneity), (2) spatial variability of soil properties (macro-heterogeneity) or (3) a combination of (1) and (2). The classical water flow theory based on the Buckingham and Darcy laws. However, when macropores are present this theory may not adequately describe the infiltration and redistribution of water as shown by **Mallants *et al.* (1996).** This behavior is described several times in literature as "channeling flow", "preferential flow", "short-circuiting" or "bypass flow" unequivocal definition of

macroporosity does not exist, in part because there are several forming processes resulting in macropores of different size, shape and continuity, and in part because the soil material (texture) has an impact (what can be seen as macropores in a fine textured clay soil, can just be a part of the bulk soil volume in a coarse textured sandy soil **(Feyen *et al*., 1998).**

Hendrickx and Flury (2001) defined preferential flow as 'all phenomena where water and solutes move along certain pathways, while bypassing a fraction of the porous matrix. Thus, an important characteristic of preferential flow is that during wetting, part of the moisture front can propagate quickly to significant depths while bypassing a large part of the matrix pore-space. Water and solutes may move to far greater depths, and much faster, than would be predicted with the Richards equation using area-averaged moisture contents and pressure heads **(Beven, 1981).** The presence of macropores and other structural features, development of flow instabilities (i.e. fingering) caused by profile heterogeneities or water repellency **(Hendrickx *et al*., 1993)**, and funneling of Flow due to the presence of sloping soil layers that redirect downward water flow are probably the most important causes of preferential flow. While the latter two processes, i.e. flow instability and funneling, are usually caused by textural differences and other factors at scales significantly larger than the pore scale, macropore flow and transport are usually generated at pore or slightly larger scales, including scales where soil structure first manifests itself (i.e. the pedon scale).

Accurate coupling of the fracture and matrix domains still represents the greatest challenge in terms of successfully describing non-equilibrium flow and transport in the vadose zone. Matrix–macropore (or matrix–fracture) interfaces can have very different properties than the bulk matrix due to the deposition of organic matter, various types of coatings, fine texture mineral particles, or various oxides and hydroxides on the aggregate exteriors or macropore walls; these coatings can markedly reduce rates of diffusion and mass flow between macropores and the soil matrix **(Thoma *et al*., 1992).**

Physical non-equilibrium occurs in the soil unsaturated zone when heterogeneity results in the generation of lateral differences (non-uniformity) either in water pressures or solute concentrations or both, during vertical flow and transport **(Jarvis, 2007).**

From the present study we need more basic research to cover the knowledge gaps according to the following points:

1- More research is clearly needed on the role and importance of long-term leaching in macropores and kinetic non-equilibrium sorption effects.
2- Further advances can be expected from researches that explain the combine geometric descriptions of soil macropores structure with continuous real-time measurements of solute transport.
3- One more working concept is that a coarser, more heterogeneous structure (associated with a decrease in macro-porosity) promotes strong non-equilibrium macropore flow but only until critical limit is reached when macropore connectivity becomes limiting. These effects of pore volume and spectral dimension may be investigated for transport by diffusion, but not with gravity-driven convective processes such as macropore flow.
4- Since any model is simplification of reality and the underlying reality is never known exactly, model simulation results are inherently uncertain. One expression of this uncertainty is equifinality, characterized by multiple model structures and parameter sets yielding acceptable fits to observed data **(Beven,**

2006). To better understand the uncertainty and limitations of the model structure, the optimization problem can be formulated in a multi-objective context, where information contained in several data-sets is exploited simultaneously **(Gupta *et al*., 1998; Vrugt *et al*., 2003; Wohling and Vrugt, 2008; Köhne *et al*., 2011).**